New biomarkers for cartilage regeneration following autologous chondrocyte transplantation

Dissertation

zur Erlangung des akademischen Grades
doctor rerum naturalium (Dr. rer. nat)

vorgelegt dem Rat der Medizinischen Fakultät
der Friedrich-Schiller-Universität Jena

von M.Sc
Pavan Kumar Kalla

geboren am **02.05.1989** in Visakhapatnam, **Republic of India**

Gutachter:

1. Prof. Dr. Raimund W. Kinne, Eisenberg
2. Prof. Dr. Reinhard Wetzker, Jena
3. Prof. Dr. Michael Sittinger, Berlin

Tag der öffentlichen Verteidigung: 29th January 2019

ABSTRACT

The present study aimed at defining biomarkers and functional pathways for the optimization of chondrogenic differentiation in stem cell-based, autologous chondrocyte transplantation (MACT). First, biomarkers and pathways of chondrogenic differentiation were defined in cartilage regenerates after MACT/cartilage repair procedures by generating an atlas of differential gene expression between second look biopsies (2^{nd} LB) and normal cartilage, osteoarthritis (OA) cartilage, or 3D-cultured chondrocytes using Affymetrix microarrays and bioinformatics. Target molecules/pathways were then validated by PCR and gene ontology analysis. The functional importance of the periostin-Wnt-MMP13 pathway was then addressed by silencing of periostin in OA chondrocytes and the analysis of target and phenotype genes at the mRNA and protein level. There was only limited similarity between 2^{nd} LB and normal cartilage, indicating incomplete repair after cartilage replacement. On the other hand, similarities between 2^{nd} LB and OA cartilage concerning the expression of inflammatory response genes suggested a contribution of inflammatory processes to the incomplete defect healing. Also, the overexpression of matrix degradation and mis-differentiation markers (including the periostin-Wnt-MMP13 pathway), indicated molecular abnormalities during insufficient cartilage repair. As a proof of concept, successful silencing of periostin in OA chondrocytes resulted in transient downregulation of tissue-degrading MMP13 (mRNA and protein) and in upregulation of cartilage-specific collagen 2, pointing to favorable effects of periostin silencing on the chondrogenic phenotype and the formation of mature cartilage. Transient upregulation of the wound healing markers ICAM 1 and collagen 3, however, indicated that periostin silencing may concurrently augment the formation of scar tissue, requiring further refinement of the therapeutic molecular targets.

ABSTRAKT

Ziel der aktuellen Studie war die Definition von Biomarkern und funktionellen Signalwegen zur Optimierung der chondrogenen Differenzierung in der Stammzell-basierten autologen Chondrozyten Implantation (MACT). Zuerst wurden Biomarker und funktionelle Signalwege der chondrogenen Differenzierung in Knorpelregeneraten nach MACT/Knorpel-Reparatur durch die Etablierung eines differenziellen Genexpressions-Atlas zwischen „second look“ Biopsien (2nd LB) sowie normalem Knorpel, Osteoarthritis (OA) Knorpel und 3D-kultivierten Chondrozyten mittels „Affymetrix microarrays“ und Bioinformatik identifiziert. Zielmoleküle/Signalwege wurden mittels PCR und „gene ontology“ Analyse validiert. Dann wurde die funktionelle Bedeutung des Periostin-Wnt-MMP13 Weges durch das „silencing” von Periostin in OA Chondrozyten und die Analyse von Ziel- und Phänotyp-Genen adressiert.

Es gab nur begrenzte Ähnlichkeiten zwischen 2nd LB und normalem Knorpel, ein Hinweis auf eine unvollständige Reparatur nach Knorpelersatz. Andererseits deuteten Ähnlichkeiten zwischen 2nd LB und OA Knorpel bei der Expression von Genen der Entzündungsreaktion auf einen Beitrag von Entzündungsprozessen zur unvollständigen Defektheilung hin. Außerdem wies die Über-Expression von Markern des Matrix-Abbaus und der Fehl-Differenzierung (inkl. des Periostin-Wnt-MMP13 Weges) auf molekulare Abnormalitäten während der insuffizienten Knorpelreparatur hin. Als „proof of concept” führte das erfolgreiche „silencing” von Periostin in OA Chondrozyten zur transienten Unterdrückung der Gewebs-abbauenden MMP13 (mRNA and protein) und Hochregulierung von Knorpel-spezifischem Kollagen 2 als Hinweis auf positive Effekte des Periostin „silencing” auf den chondrogenen Phänotyp und die Bildung von reifem Knorpel. Die transiente Hochregulierung der Wundheilungsmarker ICAM 1 und Kollagen 3 deutete jedoch an, dass das Periostin „silencing” gleichzeitig zu einer Verstärkung der Narbenbildung führt, was die Notwendigkeit zur verfeinerten Auswahl der therapeutischen Zielmoleküle belegt.

TABLE OF CONTENT

Abbreviations

2nd LB	2nd look biopsies
ACAN	Aggrecan
Bp	Base pair
COL2	Collagen 2
CXCL14	C-X-C Motif Chemokine Ligand 14
CCL18	C-C Motif Chemokine Ligand 18
CXCL8	C-X-C Motif Chemokine Ligand 8
DPT	Dermatopontin
DNA	Deoxyribonucleic acid
dNTP	deoxyribonucleotide triphosphate
E	Exon
EMC	Extracellular matrix
EDTA	Ethylenediaminetetraacetic acid
ELISA	Enzyme-linked immune sorbent assay
EGR3	Early Growth Response 3
GAPDH	Glyceraldehyde-3-phosphate dehydrogenase
ICAM 1	Intercellular adhesion molecule 1
IL	Interleukin
IF	Isoform
RPM	Revolutions per minute
LB	Lysogeny broth
MF	Microfracturing
MACT	Matrix-assisted, autologous chondrocyte transplantation
MMP	Matrix metalloproteinases
MSC	Mesenchymal stem cells
OA	Osteoarthritis
NO	Nitric oxide
PCR	Polymerase chain reaction
PENK	Proenkephalin
RNA	Ribo Nucleic Acid

SOM	Self-organizing maps
siRNA	silencing RNA
SDS-PAGE	Sodium dodecyl sulfate polyacrylamide gel
SLC7A11	Solute Carrier Family 7 Member 11
SLC5A3	Solute Carrier Family 5 Member 3
TMB	Tetramethylbenzidine
TNFRSF11B	TNF Receptor Superfamily Member 11b
TNF	Tumor necrosis factor
WISP-1	Wnt-induced signalling protein 1

Units

%	Percent
°C	Degree Celsius
µM	micromolar
µm	micrometer
A	Ampere
h	hour
l	liter
M	Molar
mA	milliampere
mg	milligram
min	minute
ml	milliliter
mM	millimolar
ng	nanogram
nm	nanometer
nM	nanomolar
rcf	relative centrifugal force
RT	Room temperature
sec	second

1 INTRODUCTION

1.1 Epidemiology of cartilage defects

Cartilage defects are one of the top ten most disabling diseases in the industrialized countries. Traumatic and osteoarthritis defects possess a very limited spontaneous regeneration capacity and often result in dramatic loss of cartilage, which may lead to partial or complete loss of joint function. This represents a therapeutic challenge, particularly in young and active individuals [1]. Such defects result in considerable pain and reduction of the quality of life for the affected individual, but also cause an enormous socioeconomic impact due to work disability and ambulatory or stationary therapy. During the past 25 years, promising new strategies have emerged using assorted scaffolds and cell treatments with expanded chondrocytes [2-4]. Current techniques for the repair of joint cartilage defects (e.g., microfracturing of the subchondral bone plate or matrix-/scaffold-assisted, autologous chondrocyte transplantation [MACT]) have so far not resulted in complete healing of the defect with the formation of fully mature (hyaline-like) cartilage. This shows the prevailing need to understand cartilage biology and the mechanisms of cartilage damage and remodeling in cartilage pathology, for example during the development of OA or aging, with the aim to improve therapeutic strategies to prevent cartilage damage and promote repair [5]. The aim of the current study was to better understand the molecular processes underlying cartilage healing by high quality, comparative molecular network analysis and the identification of key biomarkers supporting or preventing complete regeneration of the injured cartilage.

1.2 Cartilage

Cartilage, one of the main types of connective tissue, is a tough, flexible tissue that covers and protects the ends of long bones in the joints and serves as a structural component of rib cage, ear, nose, bronchial tubes, intervertebral discs, and other body components. There are three different types of cartilage in the body. Elastic cartilage is found in the ear, part of the nose, and the trachea, fibrous cartilage occurs for example in specialized cartilage pads called menisci, and hyaline or articular cartilage is found in joints, the septum of the nose, and the trachea.

1.2.1 Structure of articular cartilage

Human articular cartilage is a highly specialized tissue with a thickness of 2 to 4 mm, which provides the low-friction gliding essential for physiological joint function [6]. It consists of a dense

extracellular matrix (EMC) with sparsely distributed, specialized chondrocytes (1-5% v/v). The articular cartilage is differentiated into a thin superficial (tangential) zone which protects the deeper layers from the compressive forces (Fig. 1). Immediately below the superficial zone is the middle (transitional) zone, which acts as an anatomic and functional bridge between the superficial and deep zones. The middle zone occupies approx. 40% to 60% of the total cartilage volume and shows an increasing relative concentration of proteoglycans and a decreasing concentration of collagen, which results in decreased tensile strength and increased pressure loading capacity. The deep zone takes up approx. 30% of the articular cartilage volume and provides the greatest resistance to compressive forces. The tide mark situated beneath separates the deep zone from the calcified cartilage, which shows a scarce cell population of hypertrophic chondrocytes and plays an integral role in connecting cartilage to bone by anchoring the collagen fibrils of the deep zone in the subchondral bone (Fig. 1).

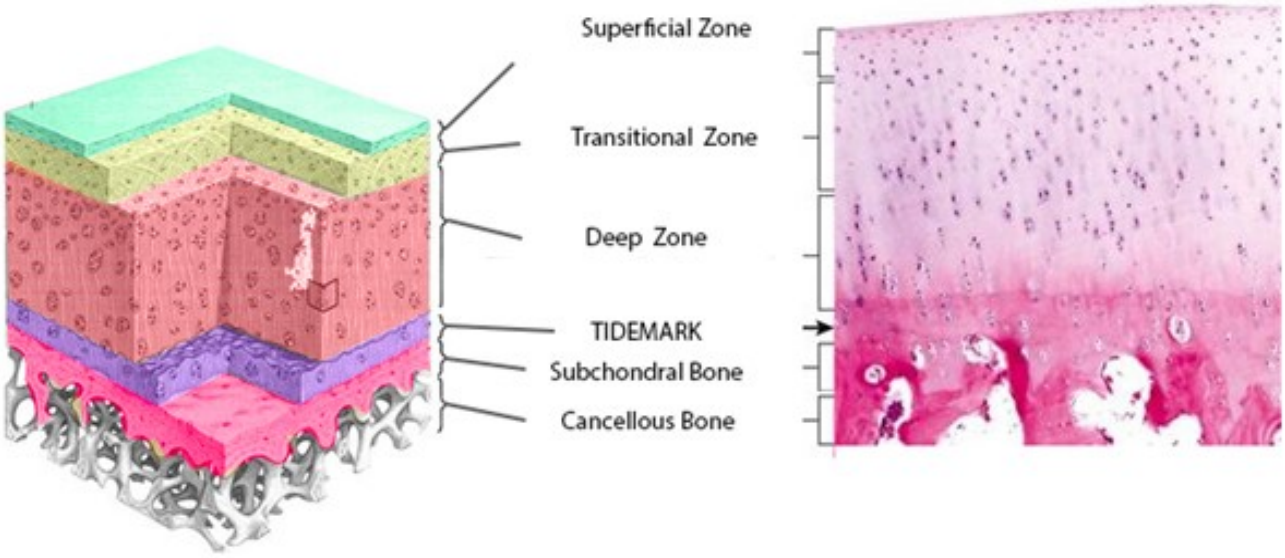

Figure 1: Principal structure of hyaline cartilage with its different layers [7].

1.2.2 Composition of articular cartilage

The extracellular matrix (ECM) of the articular cartilage contains between 65 and 80 mass % of water. This high-water content allows load-dependent deformation of the cartilage and provides nutrition and medium for lubrication, creating a low-friction gliding surface. Collagen fibers, which represent 10–20% of the wet weight of articular cartilage, are the second major component. Cartilage-specific collagen II forms the principal component of the macrofibrillar framework,

which provides tensile strength to the articular cartilage. Table 1 shows the different types and functions of the collagens found in articular and calcified cartilage [8, 9].

Collagen type	Morphological location	Function
I	Healed cartilage	Formation of calcified cartilage/scar
II	Major macrofibril component (≤ 95%)	Provision of tensile strength
III	Matrix	Matrix maturation, tissue healing
VI	Pericellular matrix	Chondrocyte-matrix attachment
V	Matrix	Component of bone matrix
IX	Cross-linked to surface of macrofibrils	Tensile strength; inter-fibrillar junctions

Table 1: Types of collagens and their functions in articular cartilage, calcified cartilage, and bone.

Proteoglycans are another major component of articular cartilage. These protein polysaccharides constitute 10–20% of its wet weight and provide compressive strength to the articular cartilage. There are two major classes of proteoglycans in articular cartilage, i.e., the large aggregating proteoglycan (aggrecan) and small proteoglycans, including decorin, biglycan, and fibromodulin. Proteoglycans are produced inside the chondrocytes and then secreted into the ECM [10]. Main functions of the chondrocytes are to synthesize various matrix components, also including dermatopontin (DPT; [11]) and to regulate the matrix metabolism [2, 12].

1.3 Cartilage degradation

Articular cartilage is devoid of blood vessels, lymphatics, and nerves and has a unique ability to withstand the high cyclic loads associated with the harsh biomechanical environment in the joint. Surprisingly, however, articular cartilage has a limited capacity for intrinsic healing and repair. Preservation and health of the articular cartilage are paramount for proper joint function. Due to its role as a cushion for bone articulation, articular cartilage is subject to many types of damaging insults, including decades of wear and tear, as well as acute joint injuries. Throughout life, the tissue undergoes continual internal remodeling as the cells replace matrix macromolecules lost through degradation [7]. When the catabolic activity is increased, lost cartilage is not completely replaced, neither quantitatively nor qualitatively. Consequently, articular cartilage progressively deteriorates and is eventually eroded, exposing the subchondral bone to the joint space, triggering

inflammation and osteophyte development, and generating severe pain and joint incapacitation [6]. This is the case in a major degenerative joint disease such as osteoarthritis (OA) [13]. There is a cascade of molecular phenomena occurring during the process of cartilage degradation.

1.3.1 Molecular Pathology of Cartilage degradation

OA strongly affects cartilage biology and leads to progressive cartilage degradation. During the development of OA, normal, quiescent chondrocytes become activated and undergo a phenotypic shift, resulting in fibrillation and degradation of cartilage matrix [14]. In healthy cartilage, chondrocytes respond to their microenvironment to maintain a delicate balance between synthesis and degradation of the ECM, the major components of which are type II collagen and aggrecan [15]. In OA, the water content in the EMC rises to more than 90% due to increased permeability and disruption of the matrix. This leads to a decreased modulus of elasticity and thus a reduction of the load bearing capability of the articular cartilage [12]. When the normal physiological mechanisms maintaining the matrix equilibrium fail, ECM components are lost, expanded chondrocytes cluster in the depleted regions, an oxidative state is induced in the stressed cellular environment, and, ultimately, chondrocyte apoptosis occurs [15-17]. Failure of the matrix equilibrium is due to increased expression of matrix-degrading enzymes [18], inhibition of matrix synthesis [19], and excessive production of pro-inflammatory mediators, such as cytokines, chemokines, and matrix degradation products [19, 20].

1.3.2 Pro-Inflammatory Cytokines

The increased production of pro-inflammatory cytokines is a typical cartilage response and one of the key factors for cartilage degeneration in OA [21]. The cytokines IL-1β, IL-6, and TNF-α play a central role in the pathogenesis and disease severity of OA. During the development of OA, the IL-1β expression in the OA synovial fluid and membrane is elevated. IL-1β strongly induces the expression and release of proteolytic enzymes, such as matrix metalloproteinases (MMPs) and aggrecanases, and suppresses the expression of ECM components, including type II collagen and aggrecan. Other inflammatory cytokines such as TNF-α promote the production of nitric oxide (NO), a potent catabolic and pro-apoptotic mediator, in the synovial tissue. The cytokines thus directly and indirectly contribute to the destruction of the structural cartilage components.

1.3.3 Proteases

Proteolytic cleavage of the major components of the cartilage extracellular matrix is executed by the 'a disintegrin and metalloproteinase with thrombospondin motifs' (ADAMTS) family members. These proteases are synthesized by chondrocytes and synovial cells in response to inflammatory stimuli. Metalloproteases are involved in the initial steps of matrix breakdown. Chondrocyte-derived matrix metalloproteinases (MMPs) and ADAMTSs family members [22] are the main enzymes involved in the breakdown of cartilage collagens and proteoglycans.

1.3.4 The MMPs

MMPs are a class of enzymes involved in the degradation of extracellular matrix molecules and in tissue remodeling. Under physiological conditions, MMP synthesis, activation, and activity are tightly regulated. For this reason, all MMPs are synthesized as inactive proenzymes. Critical pathways such as the Wnt pathway play an important role in the activation of the MMPs. For example, the Wnt-induced signalling protein 1 (WISP-1) increases the expression of MMPs.

Among the MMPs, MMP1, 8, and 13 are highly specific, since they are the only ones capable of degrading native fibrillar collagen. MMP13 is by far the most studied MMP concerning its role in cartilage, as it is the major catabolic effector in osteoarthritis and other forms of cartilage degradation, owing to its robust ability to cleave the predominant collagen type II in articular cartilage. In addition to its main target type II collagen, the enzyme also cleaves other matrix molecules such as types IV and IX collagen. If the expression of MMP13 in the joint is elevated, there is significant cartilage damage and a rapid progression of joint destruction [23]. One of the up-stream regulators of MMP13 expression during cartilage degeneration is periostin [24].

1.4 Functional roles of periostin in cartilage degradation

Periostin, also termed osteoblast-specific factor 2, is a 93 kDa, secreted, vitamin K-dependent, glutamate-containing matricellular protein. Periostin is constitutively present at low levels in most adult tissues and contributes to repair processes after injury, epithelial mesenchymal transition, as well as extracellular matrix restructuring and remodeling. Indeed, periostin is highly expressed at sites of injury or inflammation and in tumors within the adult organism and actively contributes to tissue degeneration, inflammation, fibrosis, and tumor progression (Fig. 2; [25]). For this purpose, periostin can associate with other critical extracellular matrix (ECM) regulators such as TGF-β and induce the production of pro-inflammatory chemokines [26].

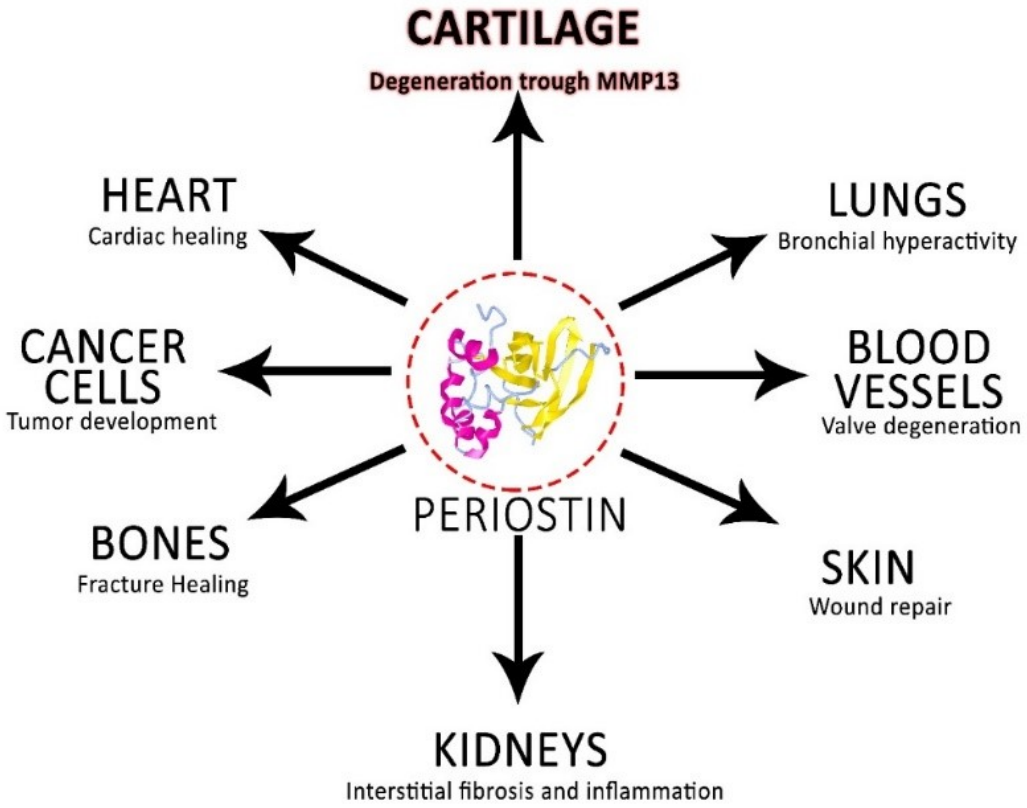

Figure 2: Functional roles of periostin in various tissues.

Periostin contributes to cartilage degeneration in OA through induction of MMP13 expression via Wnt signaling (Fig. 3A; [24, 27]). However, the molecular mechanisms underlying this process are still poorly understood. Periostin is expressed in eight isoforms, which are differentially expressed in various organs, and some of which appear to have tissue-specific functions [28-31]. This on one hand renders therapeutic targeting of periostin a complex molecular biological task, but on the other hand creates the theoretical possibility of selectively targeting cartilage-specific isoforms to prevent or reduce cartilage degeneration in OA [32]. Direct and indirect down-stream targets of periostin include MMP3 and MMP13 [24, 33], the TGF-β-interacting ECM molecule dermatopontin (DPT; [34]), the opoid polypetide hormone proenkephalin (PENK; also increased in psoriasis [35] and hypermethylated in prostate and colorectal cancer [36, 37]), and the intercellular adhesion molecule 1 (ICAM 1; Fig. 3)[38].

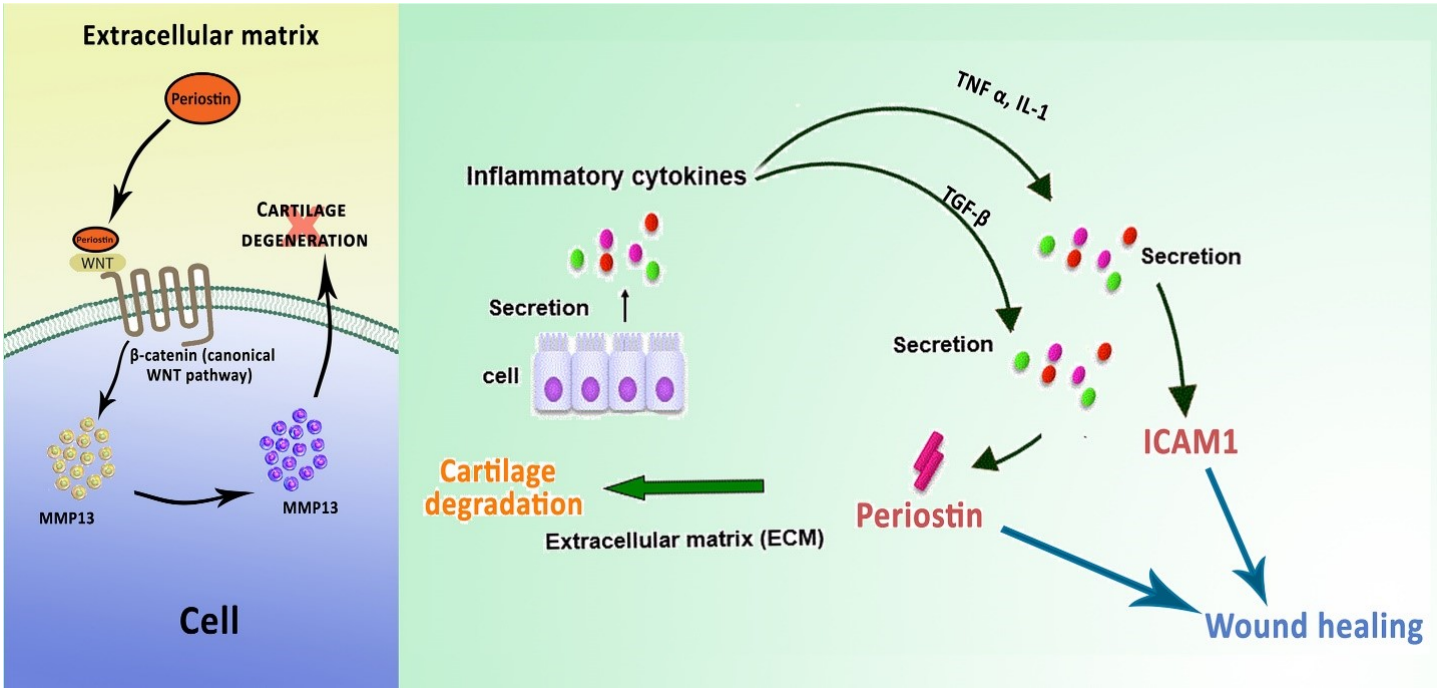

Figure 3: Periostin actions on MMP13 (via Wnt signaling) and ICAM1.

1.5 Cartilage regeneration

Unfortunately, cartilage damage in humans is not readily repaired, in part because cartilage doesn't have its own blood supply to readily provide regeneration-promoting factors. There are many novel therapeutic approaches aimed at restoring the composition, structure, and functional properties of normal human adult articular cartilage, e.g., engineering of tissue implants, use of tissue scaffolds, and application of growth and differentiation factors [4, 6, 39-43]. However, such therapies often fail to promote the formation of fully mature cartilage [6].

1.5.1 Treatment strategies

Recently, several repair techniques have been established for the treatment of cartilage lesions, e.g., cell-free (bio-engineered scaffolds, cell-free OCT from commercial banks; [1, 3, 40]), cell-based ((M)ACT, OAT), and stem cell-directed procedures (micro-abrasion, Pridie-drilling).

1.5.2 Debridement and Lavage

Debridement includes the removal of loose joint bodies and the smoothening of the cartilage surface, whereas mostly arthroscopic joint lavage eliminates up to 14 digestive, oxidative enzymes derived from chondronecrosis. However, these cleaning and rinsing techniques only ablate pain and reduce inflammation, but do not repair damaged articular cartilage [44].

1.5.3 Cartilage abrasion

This technique removes worn-out layers of the cartilage and “refreshes” the surface. It is very simple and fast, but often does not yield a sufficient long-term outcome [44].

1.5.4 Microfracturing (MF)

MF (previously Pridie-Drilling) enables mesenchymal stem cells to migrate into damaged cartilage, differentiate at this site, and build new cartilaginous tissue. However, the regenerate often does not match the properties of the original cartilage, but represents fibrocartilaginous scar tissue, questioning the ability of MF to improve cartilage regeneration [44].

1.5.5 Osteochondral autologous transplant (OAT)

An osteochondral autologous graft of the size of the defect is harvested from a region of the joint that is less exposed to mechanical strains than the original defect site. Then the graft is inserted into the defect by the press-fit technique. One advantage of this method is a very good healing rate at the insertion site. However, the damage at the harvest site and an often imperfect alignment of the tidemarks of graft and defect limit the use of this technique [45].

1.5.6 Cell-free, tissue-engineered scaffolds

Tissue-engineered scaffolds, sometimes combined with microfracturing, e.g., stem cell-based, autologous matrix-induced chondrogenesis (AMIC), are designed to imitate cartilage structure

and to support cell immigration and the formation of high-quality hyaline cartilage. Advantages of these cell-free approaches are rapid commercial availability, convenient handling, one-time operation procedures, and no need for autologous donor sites or tissue donors [46].

1.5.7 (Matrix-associated) autologous chondrocyte transplantation (M) ACT

During a first intervention, cartilage is arthroscopically harvested from the joint in an area less exposed to mechanical strain. Chondrocytes are then enzymatically liberated from the ECM and expanded in culture. Then the chondrocytes are implanted into the defect site, either by injection into a chamber below a fixed periostal flap or by seeding the cells onto a scaffold and subsequent insertion into the defect. Depending on the defect location, this can lead to very good clinical results, especially when treating defects with diameters ≥ 4 cm². However, one pitfall of this cost-intensive procedure is that it requires two interventions [39, 41, 47, 48].

2 OBJECTIVES OF THE STUDY

The aim of this project was to define biomarkers and functional pathways for the optimization of chondrogenic differentiation in stem cell-based, matrix-assisted, autologous chondrocyte transplantation (MACT). This was pursued by comparing 2nd look biopsies (2nd LB) from patients with MACT/cartilage repair procedures to normal cartilage on one hand and to bone marrow-derived, human MSC differentiating into chondrocytes on the other hand. The focus of our studies were potential deficits (e.g., de- or mis-differentiation) of successful and functional cartilage repair following MACT. For this purpose, the following steps were pursued:

- Definition of biomarkers and pathways of chondrogenic differentiation in cartilage regenerates after MACT by generating an atlas of differential gene expression between 2nd LB and normal cartilage, OA cartilage, or 3D-cultured chondrocytes using Affymetrix microarrays and self-organizing maps (SOM)
- Validation of molecules/pathways underlying impaired cartilage repair by PCR and gene ontology analysis
- Selection of the periostin-Wnt-MMP13 pathway for further functional analysis
- Assessment of the functional importance of this pathway for the de- or mis-differentiation of chondrocytes by silencing of periostin in OA chondrocytes and analysis of target and phenotype genes on the RNA and protein level
- Discussion of the potential value of this pathway for the improvement of cartilage repair and the development of novel treatments for articular cartilage defects

3 MATERIALS AND METHODS

3.1 Materials

Chemical Substance	Supplier
β-Mercaptoethanol	Sigma-Aldrich Chemie GmbH, Steinheim, Germany
Acetone	Carl Roth GmbH + Co. KG, Karlsruhe, Germany
Agarose-Gel	Invitrogen™, Carlsbad,CA, USA
Aquatex™	Merck KGaA, Darmstadt, Germany
$CaCl_2$	Roche Diagnostics GmbH, Mannheim, Germany
Eosin	Roche Diagnostics GmbH, Mannheim, Germany
Ethanol > 99.5%	Roche Diagnostics GmbH, Mannheim, Germany
Glycine	Roche Diagnostics GmbH, Mannheim, Germany
Hematoxyline	Hollborn & Söhne GmbH & Co. KG, Leipzig, Germany
HCl	Roche Diagnostics GmbH, Mannheim, Germany
KCl	Roche Diagnostics GmbH, Mannheim, Germany
KH_2PO_4	Merck KGaA, Darmstadt, Germany
Methanol	Roche Diagnostics GmbH, Mannheim, Germany
NaCl	Roche Diagnostics GmbH, Mannheim, Germany
Na_2HPO_4. $2H_2O$	Roche Diagnostics GmbH, Mannheim, Germany
Safranin- O solution	Hollborn & Söhne GmbH & Co. KG, Leipzig, Germany
SDS pellets	Roche Diagnostics GmbH, Mannheim, Germany
TRIS	Roche Diagnostics GmbH, Mannheim, Germany
Tween 20	Sigma-Aldrich Chemie GmbH, Steinheim, Germany

Table 2: List of chemicals.

Reagent/Medium	Supplier
Ampicillin	Gibco™, Thermo Scientific, Waltham, MA, USA.
Collagenase P	Roche Diagnostics GmbH, Mannheim, Germany.
EcoRI	New England Biolabs®,Hitchin, UK.
FBS- Fetal Bovine Serum	Gibco® by life technologies™, Darmstadt, Germany
Gentamicin (50 mg/mL)	Gibco™, Thermo Scientific, Waltham, MA, USA.
Lipfectimine	Roche Diagnostics GmbH, Mannheim, Germany
LightCycler® 480 SYBR Green I Master	Roche Diagnostics GmbH, Mannheim, Germany
MMP13 ELISA kit	R&D Systems; Minneapolis, MN, USA
One Shot ™ TOP10 Competent cells	Invitrogen™, Carlsbad,CA, USA.
Periostin ELISA kit	Adipogen International, Liestal, Switzerland
PerfeCTa SYBR Green SuperMix	Quanta bio, Beverly, MA , USA
PenStrep	Gibco™, Thermo Scientific, Waltham, MA, USA.
Pierce™ BCA Protein Assay Kit	Thermo Scientific, Waltham, MA, USA
Pronase E	Sigma-Aldrich, Taufkirchen, Germany.
RNeasy kit	Qiagen, Hilden, Germany.
Stealth™ RNAi ActinPosControl	Invitrogen™, Carlsbad,CA, USA.
Stealth™ RNAiNegContol Kit	Invitrogen™, Carlsbad,CA, USA.
SuperScript	Invitrogen, Karlsruhe, Germany
TOPO™ TA Cloning™ Kit	Invitrogen™, Carlsbad,CA, USA.
Trypsin-EDTA (0.05%)	Gibco™, Thermo Scientific, Waltham, MA, USA
West Femto Chemiluminescence HRP Substrate	SuperSignal™, Thermo Scientific™, Invitrogen

Table 3: List of reagents and media.

Dye/Antibody	Supplier	Cat. No.
Beta actin	R&D Systems Inc, Minneapolis, MN	937215
MPP13	R&D Systems Inc, Minneapolis, MN	87512
Periostin	Abcam, Cambridge, UK	ab152099
Secondary anti body		
anti- Rabbit IgG-HRP	Abcam, Cambridge, UK	ab6721
anti- mouse IgG-HRP	Abcam, Cambridge, UK	ab97046

Table 4: List of antibodies.

Consumable	Supplier
96 Well Microplate	Essen Bioscience Inc., Pittsfield Charter Township, MI, USA
Cap Strips, flat, PCR clean	Eppendorf AG, Hamburg, Germany
CELLSTAR® Cell culture flask	Greiner Bio-One GmbH, Frickenhausen, Germany
CELLSTAR® Multiwell plate (12 wells)	Greiner Bio-One GmbH, Frickenhausen, Germany
Cell scraper, 24 cm	TPP Techno Plastic Products AG, Trasadingen, Switzerland
Filter, 70 µm	Corning® cell strainer, Sigma-Aldrich, Taufkirchen, Germany
GeneChipR Hybridisation Oven 645	Affymetrix, Santa Clara, CA, USA
Microscope slides	Thermo Scientific, Waltham, MA, USA

Table 5: List of consumables.

Technical device/Instrument	Supplier
Affymetrix U133 Plus 2.0, GeneChip	Affymetrix, Santa Clara, CA, USA
Affymetrix Fluidics Station 450	Affymetrix, Santa Clara, CA, USA
Axiovert 25 inverse microscope	Carl Zeiss Microscopy GmbH, Jena, Germany
Cell Coulter	Beckman Coulter GmbH, Krefeld, Germany
Centrifuge 5417C	Eppendorf AG, Hamburg, Germany
Centrifuge 5415R	Eppendorf AG, Hamburg, Germany
Centrifuge 5810R	Eppendorf AG, Hamburg, Germany
CLARIOstar® microplate reader	BMG LABTECH, Orthenberg, Germany
Cell Counter	Cellometer Auto T4, Nexcelom, Massachusetts, USA
Eppendorf Mastercycler	Eppendorf, Hamburg, German
GeneChip Scanner 3000	Affymetrix, Santa Clara, CA, USA
Incubator HERAcell 240i CO_2	Thermo Scientific, Waltham, MA, USA
Mastercycler® ep realplex^4	Eppendorf AG, Hamburg, Germany
Multichannel pipette	Eppendorf AG, Hamburg, Germany
NanoDropTM 2000 Spectrophotometer	PEQLAB Biotechnology GmbH, Erlangen, Germany
PowerPac 200 power supply	Bio-Rad Laboratories, Inc., Hercules, CA, USA
Thermomixer comfort	Eppendorf AG, Hamburg, Germany
Titramax 1000 shaker	Heidolph Instruments GmbH, Schwabach, Germany
Trans-Blot Turbo Transfer System	Bio-Rad Laboratories, Inc., Hercules, CA, USA

Table 6: List of technical devices and instruments.

3.2 Patient material

3.2.1 Patient material for Affymetrix analyses

Cartilage was obtained from the knee joints of 5 OA patients who underwent joint replacement surgery (samples V4-V8; OA grade 2-3 according to Ahlbäck; Mankin score ≥ 4; [49]); normal cartilage (V1-V3 and V13-V16) was harvested from the medial and lateral femoral condyle of 7 adult multi-organ donors within 12-14 h post mortem ([49]; approved by the ethics committees of the Medical Faculties at Gothenburg University and Charité-Universitätsmedizin Berlin).

Samples V9-V12 contained 2nd LB (weight 10 to 50 mg) of patients with traumatic/degenerative cartilage defects previously treated with MACT with persistent joint swelling and/or pain (n = 4; mean follow-up approx. 3 years, median 1.6 years; see Table 19 on page 45; approved by the ethics committee of the Medical Faculty, Friedrich Schiller University Jena). Samples V17-V27 were isolated from normal cartilage [50], expanded in monolayer until the end of passage 0 (V26, V27), and then re-differentiated in 3D culture in fibrinogen for 7 days (V17, 20, 23), 14 days (V18, 21, 24) or 21 days (V19, 22, 25).

3.2.2 Patient material for silencing experiments

Tibia plateaus or femoral heads cylinders were collected under sterile conditions in phosphate-buffered saline (PBS) from six OA patients (age range 55-76 years), who underwent total knee or hip replacement surgery at the Department of Orthopedics, Jena University Hospital, Waldkrankenhaus “Rudolf Elle”, Eisenberg, Germany. Informed patient consent was obtained and the study was approved by the Ethics Committee of the Medical Faculty, Friedrich Schiller University Jena. In the cell culture laboratory, cartilage slices of approximately 4 mm^2 were carefully removed from the underlying bone, washed twice in PBS, and then digested for 1 hour at 37°C and 5% CO_2 (HERAcell 240i CO_2, Thermo scientific, Waltham, MA, USA) in a spinner flask in serum-free DMEM/F12 (DMEM/F12; Invitrogen, Karlsruhe, Germany) containing 0.1% pronase E (Sigma-Aldrich, Taufkirchen, Germany). After two further washes with pre-warmed PBS at 37°C, overnight enzymatic digestion was performed at 37°C in 0.05% collagenase P (Roche Diagnostics, Mannheim, Germany) in DMEM/F12 media supplemented with 10% fetal calf serum (FCS). Cells were separated by filtration through a 70 µm mesh sieve (Corning® cell strainer, Sigma-Aldrich, Taufkirchen, Germany) and centrifuged for 15 min at 1,500 rpm (Centrifuge 5417C). The pellet was washed in PBS containing 10% FCS and centrifuged again for 5 min at 1,500 rpm for a total of three times. Subsequently, the cells were resuspended in 1 ml

culture medium (DMEM/F12; 5% FCS; 1% Gentamicin; 5% pen/strep), counted in a Cellometer Auto T4 Bright Field Cell Counter, and then seeded into a 225 ml cell culture flask (1 x 10^7 cells/flask), with medium changes every second day. Chondrocytes were subcultured after reaching 90% confluence by incubation for 5 min at 37°C in 0.05% trypsin-EDTA (Versene, Gibco), centrifugation, and washing in PBS and used for experiments at passage 1.

3.3 Histological evaluation

3.3.1 Hematoxylin and eosin staining

Paraffin sections of the 2nd LB were cut into 6-µm sections and stained with hematoxylin (nuclei) and eosin (cytoplasm; H&E) for histolopathological evaluation [51]. The sections were deparaffinized with xylene, hydrated by passage through decreasing concentrations of alcohol (100%, 90%, 80%, 70%), dipped for 10 min in hematoxylin, blued under running tap water, stained for 10 min in eosin, and finally washed again in distilled water.

3.3.2 Safranin-O Staining

Safranin O staining was used to assess the proteoglycan content [52]. After deparaffinization and hydration, the sections were stained for 10 min with Safranin O, washed with distilled water, exposed for 10 min to Fast Green stain, and again washed with distilled water.

3.4 Labelling and microarray hybridization

Total RNA samples were hybridized to Human Genome U133 Plus 2.0 arrays using the GeneChip^R Expression 3`IVT Express Kit, GeneChip^R Hybridisation Oven 645, Affymetrix Fluidics Station 450, and GeneChip Scanner 3000 (all Affymetrix, Santa Clara, CA, USA). Data analysis was performed using MAS 5.0 (Microarray Suite statistical algorithm; Affymetrix) and observing MIAME criteria (http://www.mged.org/Workgroups/MIAME/miame.html).

3.5 Bioinformatic data analysis

Affymetrix data were pre-processed and normalized using the Bioconductor package *affy* [53]. Normalized expression data were analyzed by self-organizing maps (SOM) methods using the Bioconductor package *oposSOM* [54]. This analysis included all samples and was performed on 20 x 20 metagenes. D-cluster analysis was used to identify subsets of differentially expressed genes. Expression of these subsets in the individual samples was characterized using Gene Set Z-score (GSZ-score; ekhidna.biocenter.helsinki.fi/users/petri/public/GSZ/GSZscore.html).

3.6 Silencing of Human Periostin

Silencing of Periostin (POSTN) in human OA chondrocytes was performed using the siRNA technique and the Stealth™ RNAi ActinPosControl (12953-141; Invitrogen), with the 2 silencing constructs G05, and A02 (Table 7; Fig. 4). The Stealth™ RNAiNegContol Kit (12935-100) was used as a silencing control, an untouched water control was also maintained.

Stealth™ RNAi Actin Pos	Sequence	Targeted Periostin isoforms
Post siRNA G05	GAGACACGAGAAGAACGAACATTA	1, 2, 3, 4, 5, 8
Post siRNA A02	CCATGGGAACCAGATTGCAACAAAT	1, 2, 3, 4, 5, 6, 7, 8

Table 7: siRNA constructs (sequence and targeted periostin isoforms).

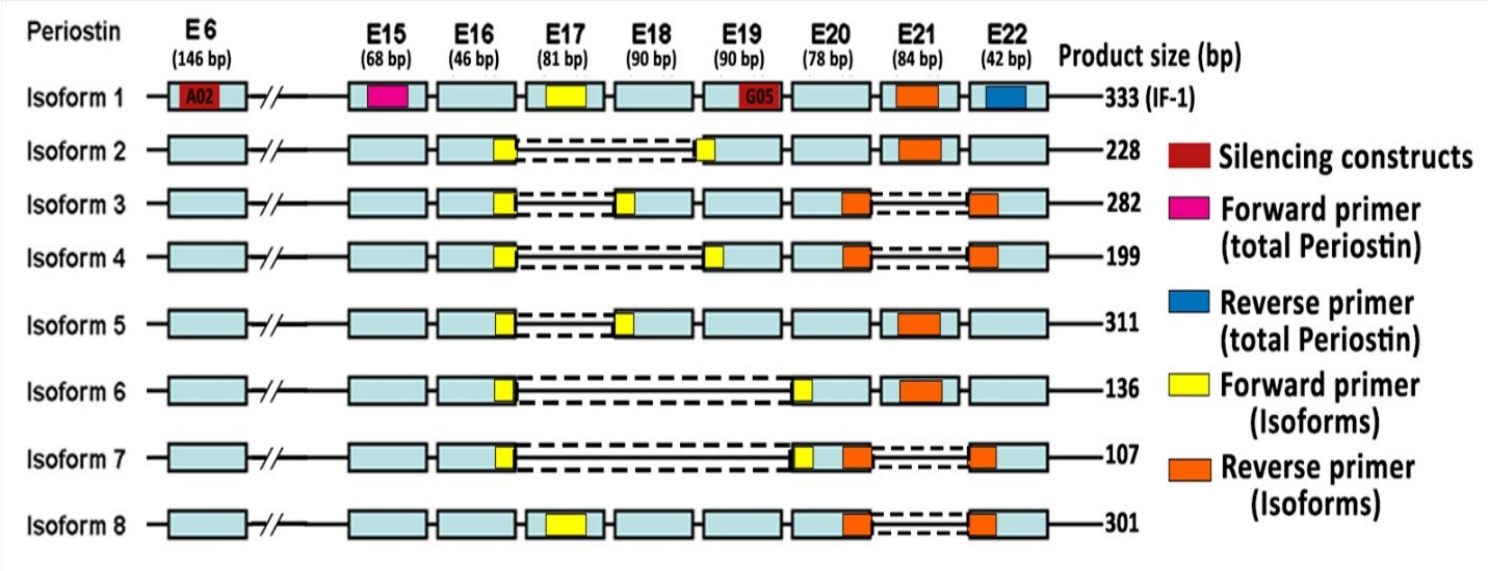

Figure 4: Position of siRNA constructs and PCR primers for periostin (total and isoforms); E = exon; bp = base pairs; IF= isoform.

For the analysis of mRNA Expression by PCR, the reagents (Table 8) were mixed and incubated for 20 min at room temperature to allow complex formation. Then 202.6 µl of the mixture were aliquoted into each well of a 12-well plate for the 2 time points (2 and 4 days), followed by addition of 1 ml each of culture medium (DMEM/F12; 10% FCS) with pre-diluted cells (2.5 x 10^5), incubation of the plates for 24 h, careful draining of the culture medium, and addition of 1 ml of

fresh culture medium (DMEM/F12; 5% FCS; 1% Gentamicin; 5% pen/strep) for 2 and 4 days. RNA was extracted and used to analyze the expression of different target and marker genes expression by PCR (see 3.6.2 below). The supernatant was stored at -80°C and later used for enzyme-linked immunosorbent assays (ELISA; see 3.8.2 below).

RNA expression silencing (two time points: 2 and 4 days)					
Reagents	**Untouched Control**	**Silencing Control**	**G06**	**G05**	**A02**
Opti-MEM®	400 µl	400 µl	400 µl	400 µl	400 µl
siRNA	1.2 µl (water)	1.2 µl	1.2 µl	1.2 µl	1.2 µl
Lipofectamine™	4 µl	4 µl	4 µl	4 µl	4 µl

Table 8: Volume of reagents required for the silencing of the RNA expression.

For the analysis of cellular protein, a five-fold volume of the reagents in Table 8 was used for the transfection of 5 x 10^5 cells for 24 h in six-centimeter petri plates with 5 ml of culture medium (DMEM/F12; 10% FCS), followed by replacement with 5 ml of fresh culture medium (DMEM/F12; 5% FCS; 1% Gentamicin; 5% pen/strep) for 2 and 4 days. Subsequently, the protein was extracted and the concentrations of MMP13 and periostin were analyzed.

3.7 RNA isolation, cDNA preparation, and real-time RT-PCR analysis

3.7.1 RNA isolation

The RNeasy kit (QIAGEN) was used to isolate the RNA. Briefly, 2.5 x 10^5 cells were lysed on ice in 350 µl lysis buffer containing 0.1% (v/v) mercaptoethanol. After centrifugation for 3 min at 10,000 rpm, the supernatant was removed carefully, 1 volume of 70% ethanol was added to the pellet, and the mixture was homogenized using a pipette. The mix was transferred to a RNeasy mini spin column, placed on a 2 ml collecting tube, and centrifuged at 8,000 rpm for 15 sec. The flow through was discarded, 700 µl RW1 buffer were added to the spin column, and the column centrifuged for 15 sec at 8,000 rpm. Then 500 µl RPE buffer were added to the spin column and centrifuged at 10,000 RPM for 1 min, followed by addition of 500 µl RPE buffer and centrifugation at 8,000 RPM for 2 min. The spin column was placed on a new 1.5 ml collecting tube and the RNA

eluted by adding 30-50 µl of RNase-free water and centrifugation at 8,000 rpm for 1 minute. The RNA concentration was measured using a nano drop spectrophotometer (NanoDropTM 2000; Thermo Fisher Scientific, Waltham, MA, USA) and stored at -80°C.

3.7.2 cDNA preparation

cDNA (20 µl) was prepared from total RNA using oligo-dT primers and SuperScript reverse transcriptase (Invitrogen, Karlsruhe, Germany). The RNA concentration was measured in a nano drop and the required RNA volume calculated by dividing 360 by the RNA concentration ($X_{ng/\mu l}$). Using a nuclease-free microcentrifuge tube, 1 µl of Oligo dt, 1 µl of dNTP MIX (10 mM each), x µl of RNA and y µl of sterile distilled water were added to result in a total volume of 12 µl. The mixture was heated to 60ºC for 5 min, quickly chilled on ice, and centrifuged for 10 sec to collect the condensate on the bottom of the tube. Then 4 µl of 5 X first strand buffer, 2 µl of 0.1 M DDT, and 1 µl of water were added, gently mixed, and incubated at 42ºC for 2 min, followed by addition of 1 µl of superscript II RT, incubation at 42ºC for 50 min, and inactivation of the enzyme by heating to 70ºC for 15 min. The cDNA was stored at -20ºC and used for RT-PCR.

3.7.3 Quantitative real-time RT-PCR analysis

In addition to cartilage and bone markers, the expression of differentially expressed genes was validated by quantitative real-time PCR in an Eppendorf Mastercycler (Eppendorf, Hamburg, Germany). The expression levels of mRNA were normalized to the expression of glyceraldehyde-3-phosphate dehydrogenase (GAPDH). PCR reaction was performed in a total volume of 20 µl. The mix was prepared (Table 9) and the mRNA expression was analyzed using a PCR machine (Eppendorf, Hamburg, Germany).

RT PCR Master Mix	
Reagent	**Amount**
PerfeCTa SYBR® Green FastMix	10 µl
RNase-Free Water	8.2 µl
Forward primer	0.4 µl
Reverse primer	0.4 µl
cDNA	1 µl

Table 9: Master mix preparation for 20 µl reaction.

Forward and reverse primers (Jena Bioscience GmbH), product size, annealing and melting temperatures for all genes are shown in Table 10. The CT values of the genes were analyzed using 2-ΔΔCT method [55].

Gene symbol	Sequence		Primers (5′–3′)	Product size (bp)	Annealing temperature, ˚C	Melting temperature, ˚C
GAPDH	NM_001289746.1	Forward	CGGAGTCAACGGATTTGG	307	60	80
		Reverse	AGCCTTCTCCATGGTGGTG			
MMP13	NM_002427.3	Forward	CACCGGCAAAAGCCACTTTA	119	60	80
		Reverse	GGTCACATTTGTCTGGCGTT			
Total Periostin (POSTN) **Isoforms (IF) 1-8**	NM_006475.2	Forward	CAGCAGACACACCTGTTGGA	622 (IF 1) 451 (IF 2) 457 (IF 3) 367 (IF 4) 541 (IF 5) 361 (IF 6) 277 (IF 7) 538 (IF 8)	60	68
		Reverse	CACTGAGAACGACCTTCCCT			
Periostin Isoform 1	NM_006475.2	Forward	AGGCAGTCTTCAGCCTATTATCA	333	60	68
		Reverse	TGACCATCACCACCTTCAATG			
Periostin Isoform 2	NM_001135934.1	Forward	CCCCGTGACTGTCTATAAGCC	228	62	68
		Reverse	TGACCATCACCACCTTCAATG			
Periostin Isoform 3	NM_001135935.1	Forward	ACTGTCTATAGACCCACAC	282	62	68
		Reverse	CCTCACGGGTGTGTCTTCTTG			
Periostin Isoform 4	NM_001135936.1	Forward	CCCCGTGACTGTCTATAAGCC	199	62	68
		Reverse	CCTCACGGGTGTGTCTTCTTG			
Periostin Isoform 5	NM_001286665.1	Forward	ACTGTCTATAGACCCACAC	311	62	68
		Reverse	TGACCATCACCACCTTCAATG			
Periostin Isoform 6	NM_001286666.1	Forward	CCGTAGCTGTCTATAGTCCTCA	136	62	68
		Reverse	TGACCATCACCACCTTCAATG			
Periostin Isoform 7	NM_001286667.1	Forward	CCGTAGCTGTCTATAGTCCTCA	107	62	68

		Reverse	CCTCACGGGTGTGTCTTCTTG			
Periostin Isoform 8	NM_001330517.1	Forward	AGGCAGTCTTCAGCCTATTATCA	301	62	68
		Reverse	CACGGGTGTGTCTTCTTGTAAC			
MMP3	NM_002422.4	Forward	TGAGGACACCAGCATGAACC	248	60	81
		Reverse	ACTTCGGGATGCCAGGAAA			
DPT	NM_001937.4	Forward	CAGGATTCCAGAGCCGCTAC	92	60	80
		Reverse	GCAGGAATATGGGCACCTCT			
PENK	NM_001135690.2	Forward	TCCTGGCTTGCGTAATGGAA	148	60	80
		Reverse	TGGCTTTCTTCCGGTTTGCT			
ICAM1	NM_000201.2	Forward	CCTTCCTCACCGTGTACTGG	92	60	80
		Reverse	GCAGCGTAGGGTAAGGTTCT			
COL1A1	XM_005257059.4	Forward	TGGAGCAAGAGGCGAGAG	122	60	80
		Reverse	CACCAGCATCACCCTTAGC			
COL2A1	XM_017018831.1	Forward	CAACCAGGACCAAAGGGACA	252	60	80
		Reverse	CTGGGCAGCAAAGTTTCCAC			
COL3A1	NM_000090.3	Forward	CGCCCTCCTAATGGTCAAGG	161	60	80
		Reverse	TTCTGAGGACCAGTAGGGCA			
COL5A1	NM_000093.4	Forward	CTACGTGGACTACGCGGAC	286	60	80
		Reverse	CCAAGAAGTGATTCTGGCCCC			
COL9A2	XM_011540717.2	Forward	AGGGCCTTCCTGGATTCTCT	219	60	80
		Reverse	CCTTGTCTCCTTTGACGCCT			
ACAN	XM_017021987.1	Forward	TGCATTCCACGAAGCTAACCT	82	60	80
		Reverse	CGCCTCGCCTTCTTGAAAT			

Table 10: Primer pairs for target and marker genes and PCR conditions (product size, annealing temperature, melting temperature).

3.8 Clonal analysis of the periostin isoform frequency in OA chondrocytes

3.8.1 Ligation

Ligation is the joining of two nucleic acid fragments by an enzyme. A sticky end ligation of the total periostin PCR product was performed using the TOPO™ TA Cloning™ Kit (Invitrogen). The amount of PCR product required for ligation depends on its DNA concentration. The reagents (Table 11) were mixed and the ligation mixture was incubated at 11ºC overnight.

Reagent	**Amount**
Total Periostin PCR Product	0.5–4 µL
Sterile Water	add to a total volume of 4 µL
Salt Solution	1 µL
TOPO® Vector	1 µL
Final Volume	**6 µL**

Table 11: **Volume of reagents required for ligation of PCR product.**

3.8.2 Transformation

Competent cells (One Shot ™ TOP10 Chemically Competent E. coli, Invitrogen) were thawed on ice for 10 min, mixed with the ligation product, and again incubated on ice for 1 h. The cells were then subjected to a heat shock at 42ºC for 20 sec and quickly returned to ice. Preheated SOC medium (250 µl; Invitrogen) was added and incubated on a heating block at 37ºC for 1 h. Subsequently, the cells were centrifuged at 10,000 RPM for 10 sec, the medium exceeding 70 µl was tipped off from the tube, the pellet was mixed with SOC medium and plated on an LB agar+ampicillin (10000:1; v/v) petri plate (Table 12).

LB agar medium - Mix at (60ºC)	
Reagent	**Amount**
Tryptone	10 g
Yeast extract	5 g
NaCl	10 g
Agar	15 g
H_2O	1 Liter

Table 12: Reagents required for the preparation of Lysogeny broth (LB) agar medium.

3.8.3 Liquid bacterial culture for Mini Prep

The colonies were picked using a sterile pipette tip and swabbed on to a new LB agar+amp (10000:1) plate. The pipette tip was then dropped into a glass test tube with 2 ml liquid broth+amp (Table 13) and incubated in a shaker incubator (*Incubator 1000* © Heidolph Instruments GmbH) at 37ºC for 16 h.

LB medium – Mix at (45ºC)	
Reagent	**Amount**
Tryptone	10 g
Yeast extract	5 g
NaCl	10 g
H_2O	1 Liter

Table 13: **Reagents required for the preparation of Lysogeny broth (LB) medium.**

3.8.4 Purification of Plasmid DNA

The liquid miniprep culture was centrifuged at 13,000 rpm for 1 min and the pellet resuspended in 100 µl of 50 mm TRIS/10 mm EDTA + rnase (4ºC). Then 200 µl of 0.2 M NAOH/1% SDS was added, followed by 150 µl potassium acetate (1 M) and the mixture was shaken vigorously and then centrifuged at 13,000 rpm for 5 min. The supernatant was transferred into a tube with 700 µl of isopropanol (4ºC) and centrifuged at 13,000 RPM for 10 min. The pellet was resuspended in 300 µl of 70% ethanol and centrifuged at 13,000 RPM for 2 min, followed by drying for 5 min. The pellet was resuspended in 50 µl of water and the DNA concentration was measured.

3.8.5 Restriction digestion

Restriction digestion is an enzymatic technique to cleave DNA molecules at specific sequences. The purified plasmid DNA was tested for the frequency of periostin isoforms. The enzyme EcoRI (New England Biolabs®) was used to cleave the plasmid DNA. The nucleic acid recognition sequence of the enzyme is G/AATTC, which has a palindromic, complementary sequence of CTTAA/G. The reagents were mixed with the plasmid sample (Table 14) and incubated at 37ºC.

EcoR1 Restriction digestion at (37°C)	
Reagent	**Amount**
Restriction enzyme	1 µl
DNA	7 µl
10 X NE buffer	2 µl
Incubation time	1 h

Table 14: **Volume of reagents required for restriction digestion.**

After restriction digestion, 2 µl of gel loading dye were added and the sample was run on a 2% agarose gel at 100 volts for 30 min. Product sizes were determined using a 1 kD DNA ladder. Some of the periostin isoforms have EcoR1 sites in the center of the PCR product (Table 15).

Periostin ISOFORMS				
Isoform	**EcoR1 Site**	**Base Pairs (bp) before EcoR1 site**	**Base Pairs after EcoR1 site**	**Product length (bp)**
Isoform 1	Present	240	382	622
Isoform 2	Absent	-	-	451
Isoform 3	Present	159	293	457
Isoform 4	Absent	-	-	367
Isoform 5	Present	159	382	541
Isoform 6	Absent	-	-	361
Isoform 7	Absent	-	-	277
Isoform 8	Present	240	298	538

Table 15: Properties of all isoforms present in the total periostin PCR product.

3.9 Protein isolation and quantification

After cultivation for 2 and 4 days, the cell plates were put on ice, washed thrice with ice-cold PBS, and incubated for 10 min with 350 µl of lysis buffer (50 mM Tris-Ci, pH 8.0, 150 mM NaCl, 1% Nonidet P40). The sample was scraped, collected into a 1.5 ml tube, and stored at -20°C.

3.9.1 BCA Protein Assay

Protein content was determined using the bicinchoninic acid assay (BCA; Pierce, Thermo Scientific, Waltham, MA, USA) following acetone precipitation of a 25 µl sample aliquot on ice for 30 min. Samples were centrifuged for 10 min at 13,000, the pellet resuspended in 50 µl of 0.1 N NaOH, and then incubated on a hot plate at 60°C for 20 min under shaking (350 rpm). Tubes were spun briefly and loaded in 96-well plates. After addition of 200 µl color agent to samples and standard, the plate was incubated for 30 min at 37°C, cooled to room temperature, and measured at 562 nm.

3.9.2 Enzyme-linked immunosorbent assay (ELISA)

ELISAs are plate-based assays for detecting and quantifying peptides and proteins.

3.9.3 Detection of Periostin

Periostin concentrations in culture supernatants were measured using a competitive periostin ELISA kit (Cat. No. AG-45B-0004-KI01; Adipogen International, Liestal, Switzerland). Different dilutions of standard and diluted samples (100 µl each) were added in duplicate into 16-well strips, the plate was covered with adhesive strips and incubated for 2 hours at 37°C. Following aspiration of the liquid, 300 µl of 1 X wash buffer were added for 5 consecutive times. Then 100 µl of diluted detection antibody were added to each well, the plate was covered with adhesive strips and again incubated for 1 hour at 37°C, followed by 5 times washing in 300 µl of 1 X wash buffer. Subsequently, 100 µl of TMB substrate solution were added, and the color reaction was developed by incubation at RT in the dark for 10-20 minutes without covering the plate. After addition of 50 µl stop solution, the optical density was determined at an OD of 450 nm using a microplate reader.

3.9.4 Detection of MMP13

MMP13 levels were measured by ELISA (Cat. No DY511; R&D Systems; Minneapolis, MN, USA). A 96-well plate was coated with diluted capture antibody overnight at room temperature (100 µl per well). After washing thrice with 400 µl wash buffer, the plate was blocked by adding 300 µl of reagent dilution to each well, covered with an adhesive strip, and incubated for 1 hour at room temperature. After washing, each well was incubated for 2 hours at room temperature with 100 µl of sample or serially diluted standard. After washing, 100 µl of detection antibody were added and the plate incubated for 2 hours at room temperature. Finally, 100 µl of Streptavidin-HRP/well were added and the plate incubated for 20 min at room temperature in the dark. After adding 50 µl stop solution, the optical density at 450 nm was determined.

3.9.5 Western blot

Western blotting, a technique to identify specific proteins in a mixture of cellular proteins, consists of: 1) size separation by denaturing SDS-PAGE (7%), 2) transfer to a solid support by electrotransfer, 3) detection of proteins with specific primary antibodies (Tables 16, 17).

Table Gel Preparation

	7% Run gel	Stacking gel
Distilled water	5.05 ml	2.95 ml
1.5 M Tris- HCL pH 8.8	2.5 ml	-
0.5 M Tris- HCL pH 6.8	-	1.25 ml
10% (w/v) SDS	0.1 ml	0.05 ml
Acrylamide/ Bisacrylmide (30%/ 0.8% w/v); Rotiphorese 30	2.6 ml	0.75 ml
10% (w/v) Ammonium pre sulphate (APS)	0.05 ml	0.04 ml
TEMED (Starter)	0.005 ml	0.01 ml

Table 16: Reagents required for the preparation of SDS-PAGE.

Separation of proteins by size was done in 7% sodium dodecyl sulfate polyacrylamide gel electrophoresis (SDS-PAGE), by incubating the sample with loading buffer at 95ºC for 5 min, centrifugation at 10,000 RPM for 10 sec, and running the processed samples on the gel at 100 volts for approximately an hour, or until the dye front ran close to the bottom of the gel.

10X TBS buffer	
Tris base	200 mM
NaCl	1.37M
TBS-T washing buffer	
10× TBS buffer	100 ml/l
Tween 20	1 ml/l
10X Tris-Glycine Transfer Buffer	
Tris	10.25 M
Glycine	1.92 M
SDS (optional)	10.2%
1X Transfer Buffer (1 Liter)	

10 X transfer Buffer	100 ml
Methanol	200 ml
Distilled H_2O	700 ml
Blocking buffer	
Milk	5%
10× TBS buffer	100 ml/l
Tween 20	1 ml/l
Stripping buffer	
β-Mercaptoethanol	50 mM
SDS	2%
Tris HCl (pH 6.7)	62.5 mM

Table 17: Buffers for Western blot analysis.

3.9.6 Electrotransfer

Proteins were transferred at 4°C onto a polyvinylidene fluoride membrane by electrotransfer for 60 min at 400 milliamperes in a transfer tank containing transfer buffer (Table 17).

3.9.7 Blocking and antibody incubation

Detection of proteins of interest was performed using specific antibodies diluted in blocking buffer (Tables 17, 18). Blotted membranes were first placed on a horizontal shaker in blocking buffer for 1 h at RT, followed by an overnight incubation at 4°C with the primary antibodies against periostin (Table 18) and MMP13 (Table 18). After washing for three times in TBS-T washing buffer for 10 min each to remove unbound antibodies, the membranes were incubated in the corresponding HRP-coupled secondary antibodies for 1 h at RT (Table 18). After another washing step, protein bands were detected using West Femto Chemiluminescence (SuperSignal™, Thermo Scientific™, Invitrogen) and visualized on a Bio-Rad Fluor-S MultiImager. Developed blots were semi-quantitatively analyzed using the ImageJ 1.50e software (Wayne Rasband, National Institutes of Health, USA).

Table Antibody dilutions

Antibody	Source, Type	Dilution
Primary antibodies		
Periostin	Rabbit, polyclonal	1: 500
MMP13	Mouse, monoclonal	1: 500
ß actin	Mouse, monoclonal	1: 4000
Secondary antibodies		
anti- Rabbit IgG-HRP	Rabbit, polyclonal	1:1000
anti- mouse IgG-HRP	Mouse, monoclonal	1:1000

Table 18: Primary and secondary antibodies and their dilutions for western blot analysis.

3.9.8 Re-hybridization of membranes

The membranes were re-probed to detect the control protein ß actin (Table 18). After removing the antibodies of the first immunoblotting in stripping buffer for 10 min at 60°C and subsequent washing in TBS-T buffer (3 x; 10 min each), the membranes were blocked and probed with the primary and secondary antibodies for ß actin as described above (Table 18).

3.10 Statistical analysis

Data were expressed as medians ± 25^{th}/75^{th} and 5^{th}/95^{th} percentiles using box plots. Significance was tested using the non-parametric Kruskall-Wallis and Mann-Whitney U tests for the 2^{nd} LB and the Wilcoxon test for the expression of silencing constructs (IBM SPSS Statistics 21 program; $p \leq 0.05$).

4 RESULTS

4.1 Histological analysis of second look biopsies

Second look biopsies (2nd LB) were obtained from patients with traumatic/degenerative cartilage defects who had undergone cartilage repair treatments such as ACT or MACT (n= 4; samples V9-V12; Table 15). The patients displayed symptoms such as persistent joint swelling and/or pain, and the 2nd LB were taken during revision surgery.

Sample No	Gender (m/f)	Age (years)	Follow-up (years)	Pathology	Type of therapy/ defect size (mm)	Location/ ICRS grade	Indication for 2nd look biopsy	Histology
V9	f	38	0.33 (4 months)	Gonarthrosis/ reactive arthritis	MACT (CaReS)/ 3.5 x 2 cm (7 cm^2)	Medial femur condyle; left/ Grade IV	Persistent crepitation; Recurrent swelling	Connective tissue SO -
V10	m	17	2.8 (2 years, 10 months)	Osteochondrosis dissecans	ACT (Periostal flap)/ 2 x 2 cm (4 cm^2)	Lateral femur condyle; left/ Grade IV	Femoropatellar pain	Degenerated cartilage SO +
V11	f	47	0.42 (5 months)	Trauma/ gonarthrosis	MACT (CaReS)/ 5 cm^2	Retropatellar; left/ Grade IV	Persistent swelling and pain	Connective tissue SO -
V12	f	52	8.0	Chondropathy	MACT/ 1 - 4 cm^2	Medial femur condyle; right/ Grade IV	Persistent swelling and pain	Degenerated cartilage/ connective tissue SO (+)

Table 19: Characteristics of the patients with 2nd look biopsies.

The 2nd LB were first histologically characterized using hematoxylin-eosin (H&E) and Safranin O staining (SO).

H&E staining of sample V9 showed characteristics of connective tissue rather than cartilage (Fig. 5A), i.e., fibroblast morphology with a long, extended shape of nuclei and cytoplasm. The 20 X magnification showed regions with abundant EMC, partially organized in a concentric fashion (Fig. 5A). SO staining in the sample was completely negative (Fig. 5B).

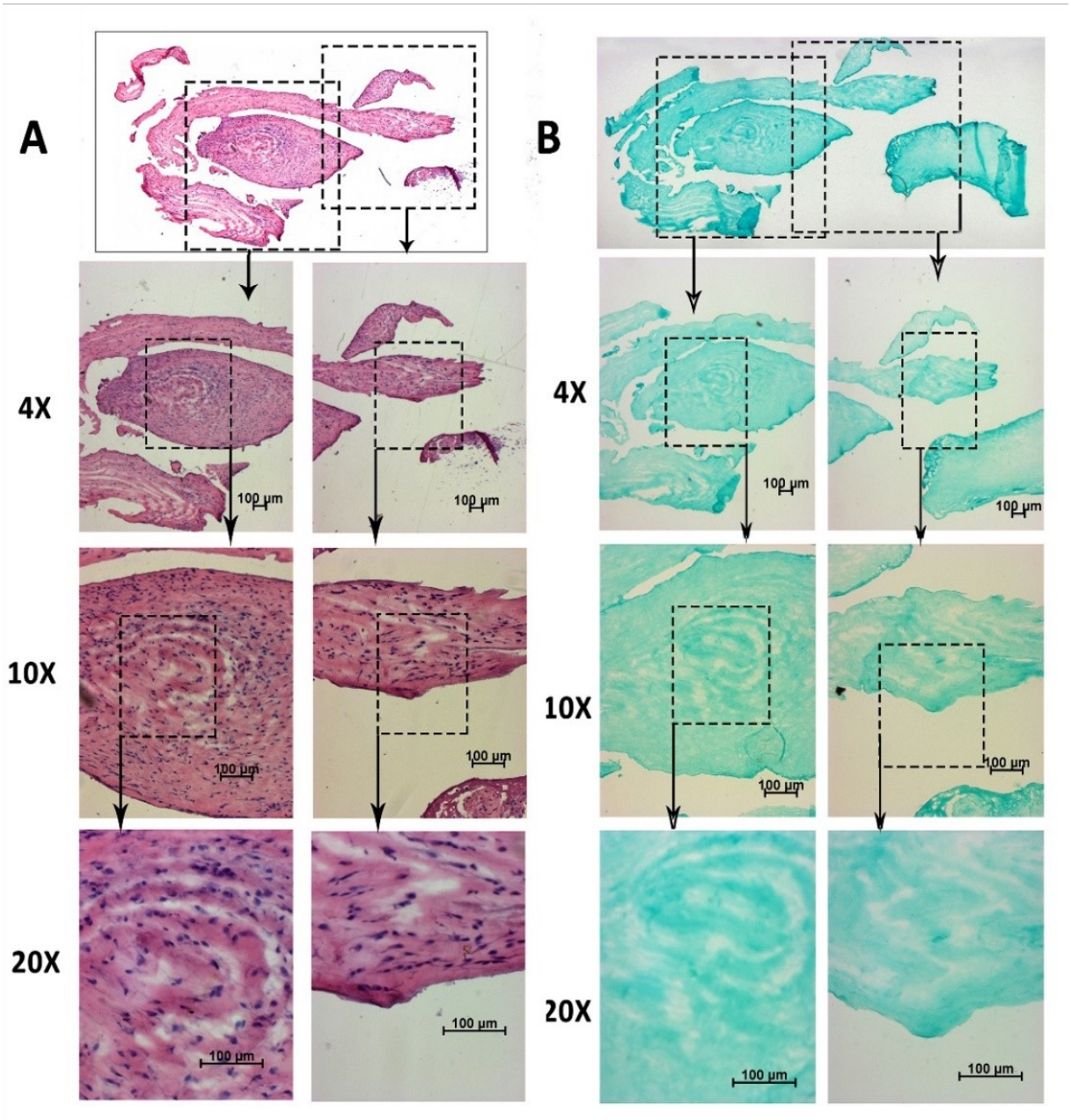

Figure 5: H&E (A) and SO staining (B) of 2nd LB sample V9.

H&E staining of sample V10 showed a high proportion of cartilage with marginal destruction and attached parts of connective tissue (Fig. 6A; overview and 4 X magnification). The 10 X and 20 X magnifications displayed partially normal cartilage, but also regions of proliferating chondrocytes clusters as a sign of cartilage degeneration (or regeneration attempts) typical of progressive OA. There was a strong red staining with SO throughout most of the cartilage, indicating a mostly preserved, high content of charged molecules such as proteoglycans. Connective tissue regions were only counterstained in green (Fig. 6B).

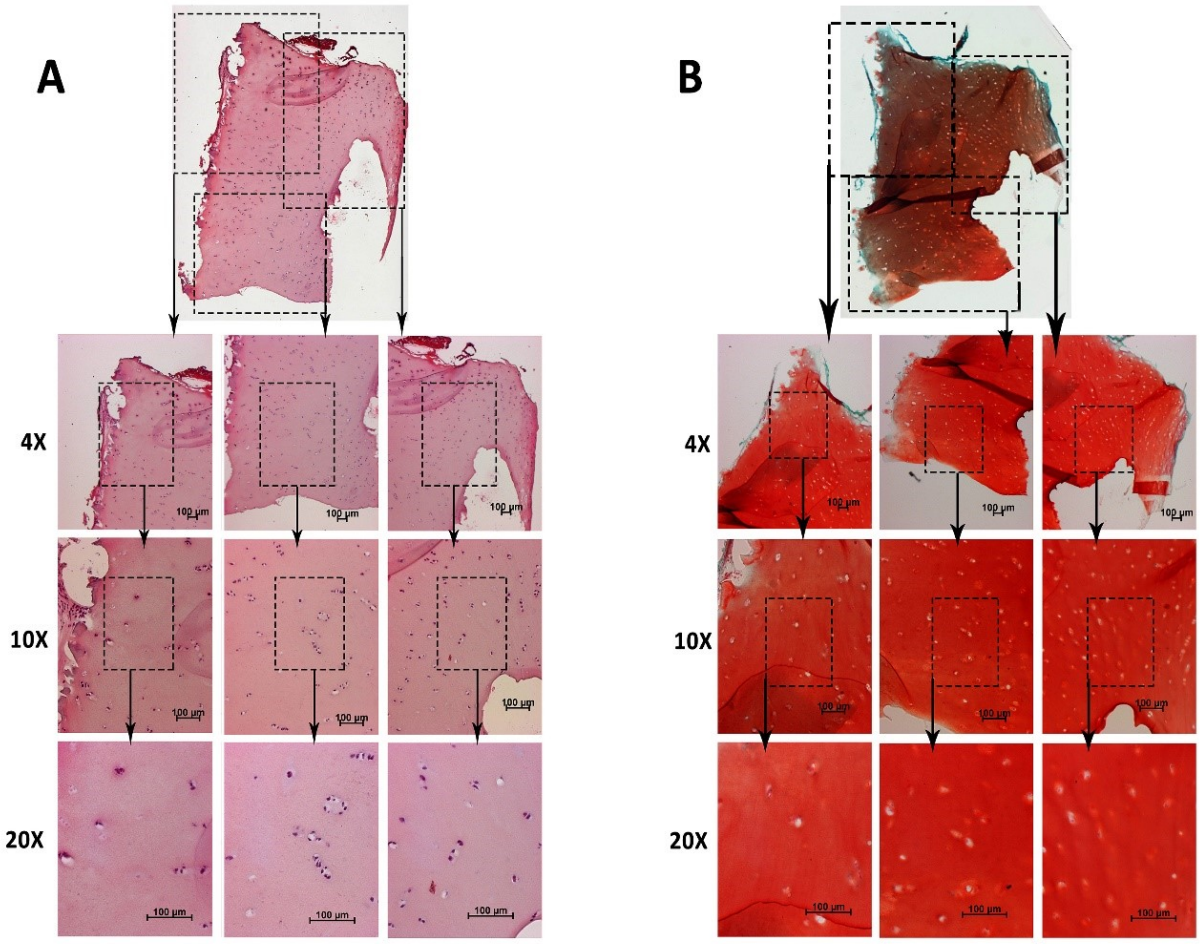

Figure 6: H&E (A) and SO staining (B) of 2nd LB sample V10.

H&E staining of sample V11 showed clear characteristics of pure connective tissue containing condensed, perivascular accumulations of mononuclear cells (Fig. 7A; in particular 10 X and 20 X). Negative SO staining confirmed the connective tissue character (Fig. 7B).

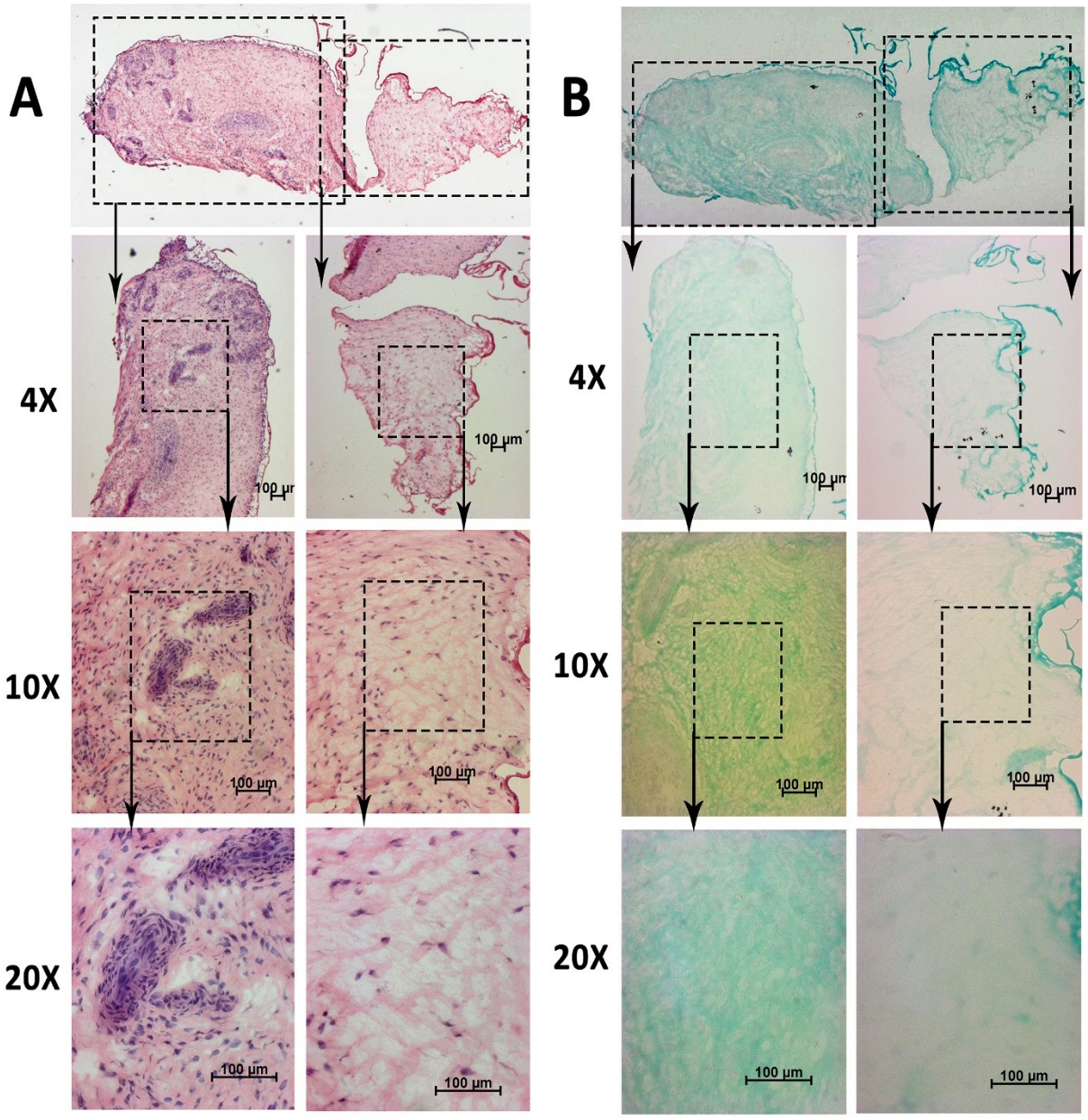

Figure 7: H&E (A) and SO staining (B) of 2nd LB sample V11.

H&E staining of sample V12 showed both cartilaginous regions and attached connective tissue regions (Fig. 8A). The connective tissue was partially surrounding and partially intruding the cartilage (Fig. 8A; in particular 4 X), similar to the cartilage destruction by the inflamed synovial membrane in OA and rheumatoid arthritis. The cartilage contained both seemingly normal regions and areas with proliferating chondrocyte clusters (Fig. 8A; in particular 20 X). Except for individual, positively stained chondrocyte nuclei, SO staining was negative (Fig. 8B).

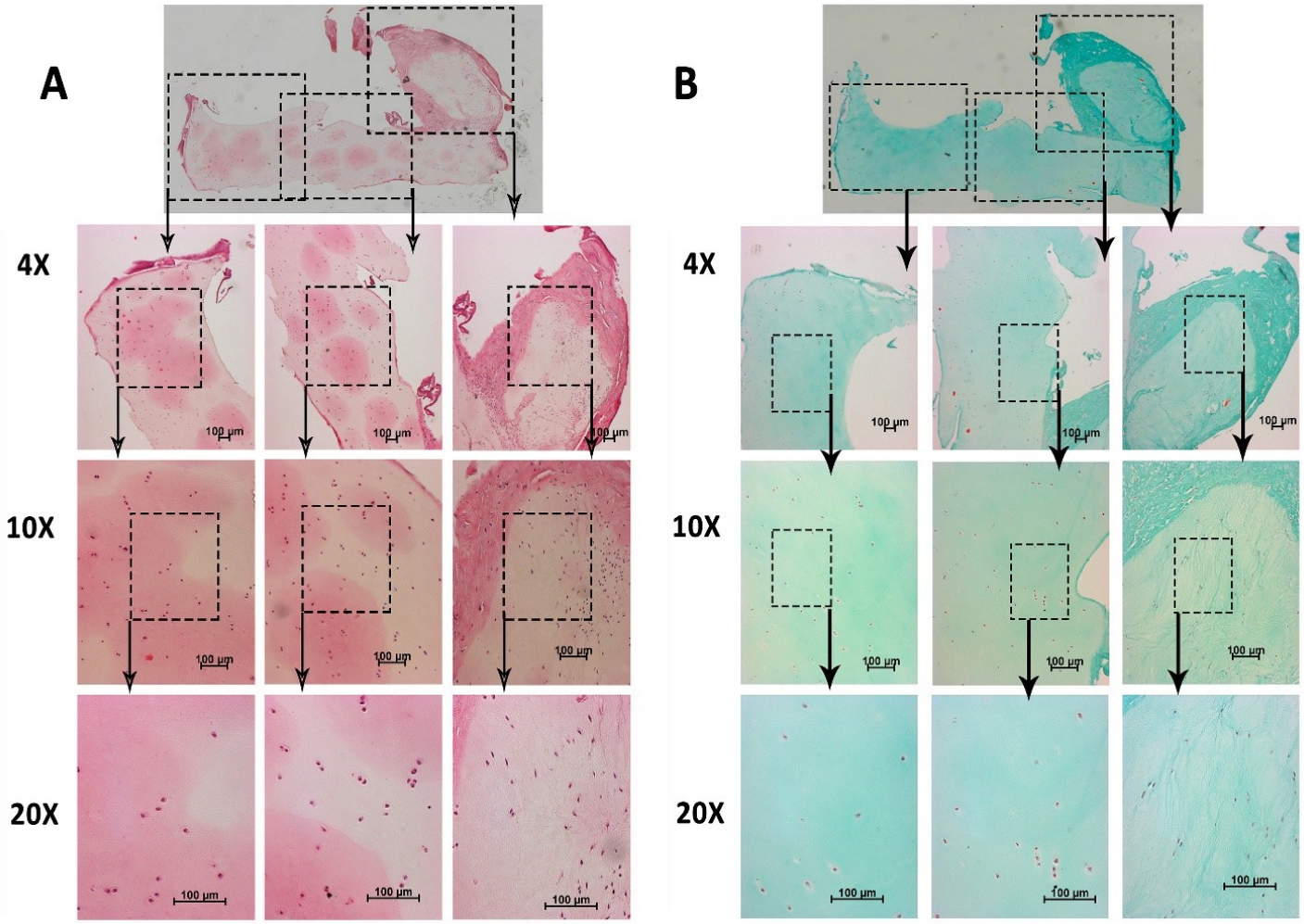

Figure 8: H&E (A) and SO staining (B) of 2nd LB sample V12.

4.2 SOM expression portraits

SOM expression portraits were generated using the complete set of Affymetrix expression data (Fig. 9). D-cluster analysis of the SOM provided 7 clusters defining gene subsets containing between 183 and 740 genes. These sets were differentially expressed in 2nd LB, normal cartilage (tissue), OA cartilage (tissue), and 3D-cultured chondrocytes from normal cartilage (Fig. 9).

Gene clusters S1 to S3 were similarly expressed in normal cartilage and 2nd LB. Set S1 distinguished all cartilage tissue samples from 3D-cultured chondrocytes (up-regulation in cultured chondrocytes) and included cellular transporter genes (SLC7A11, SLC5A3). Set S2 included genes down-regulated in 2nd LB (V9-V12) and normal cartilage (samples V13 to V16), e.g., transcription factors (e.g., RUNX1), genes influencing cartilage structural integrity (e.g., integrin-binding sialoprotein, carboanhydrase 2, microfibrillar associated protein 3), and inflammatory genes (e.g., CXCL14). Set S3 contained genes upregulated in 2nd LB and normal cartilage, which regulate chondrocyte development (e.g., insulin-like growth factor 1 receptor).

Gene clusters S4 to S7 were differentially expressed in normal cartilage and 2nd LB, with an up-regulation (S4, S5, S6) or down-regulation in 2nd LB (S7). Set S4 showed similarities of gene regulation in OA cartilage and 2nd LB, included several inflammatory genes (MHC-II molecules, macrophage markers, and chemokines such as CCL18, CXCL8), and showed large overlap with the GO gene set “inflammatory response” (not shown). Set S5 included genes interacting with the extracellular matrix (PALLD, MFAP5) and transcription factors (SOX18), and Set S6 contained interesting markers involved in matrix degradation (MMP7, MMP13, periostin), matrix regeneration (DPT, PENK) and mis-differentiation (collagens 1 and 10 alpha 1). This set showed considerable overlap with the GO gene set “extracellular matrix” (Fig. 10A, B). Expression of the genes in this GO gene set distinguished 2nd LB from normal cartilage (tissue) and chondrocytes cultured in monolayer for 0 days (Fig. 9, 10). Set S7 included genes regulating tissue architecture during wound healing (thrombomodulin, ICAM1, TNFRSF11B, EGR3, WIF1).

Thus, 2nd LB showed some similarities, but also considerable differences compared to normal cartilage and, also, shared some features with OA cartilage and 3D-cultured chondrocytes.

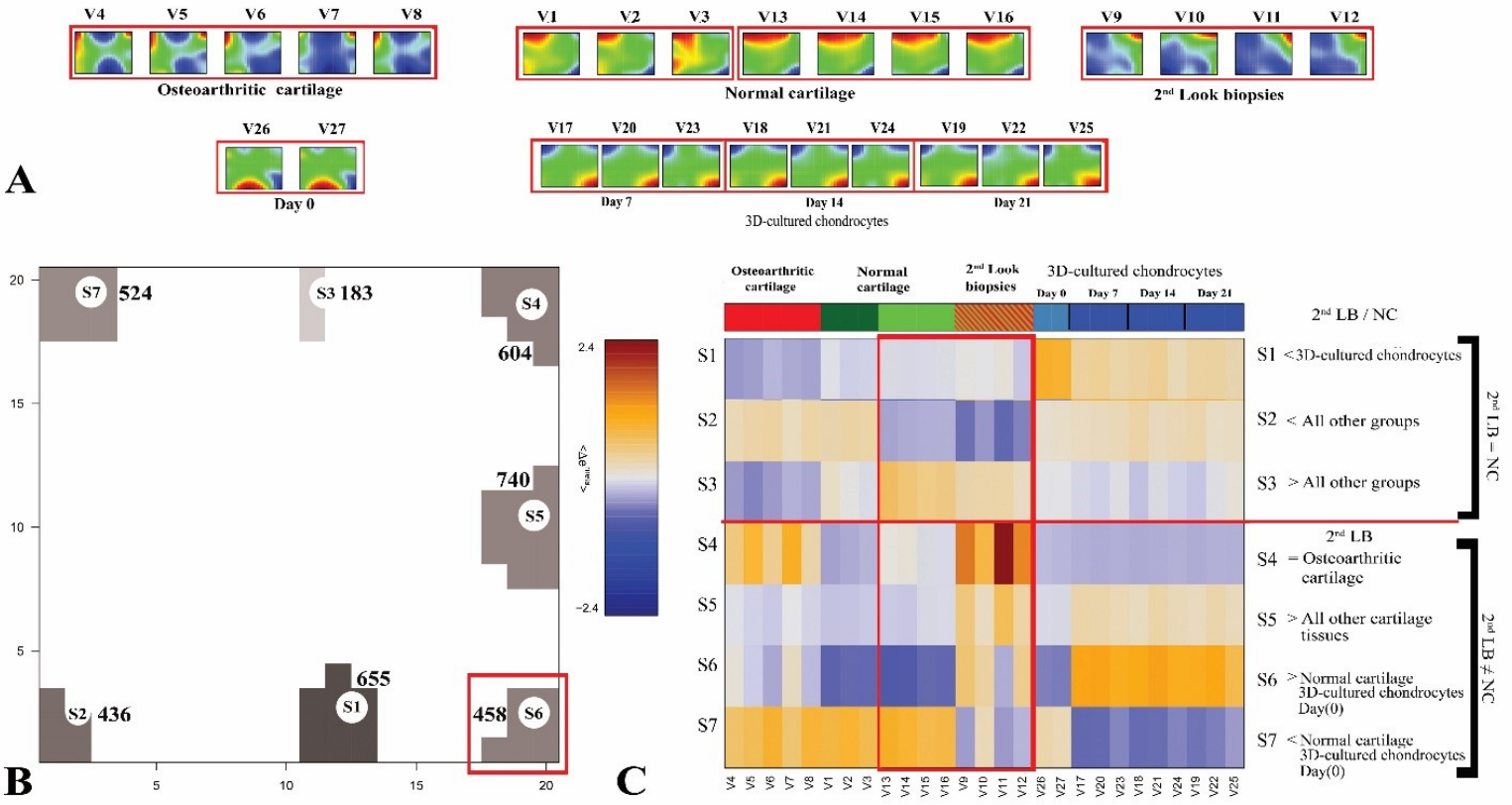

Figure 9: SOM analysis of the Affymetrix chip data. A) SOM portraits of osteoarthritic cartilage (V4 to V8), normal cartilage (V1 to V3 and V13 to V16), 2nd LB following MACT (V9 to V12), and chondrocytes expanded in monolayer until the end of passage 0 (V26, V27), and then re-differentiated in 3D culture in fibrinogen for 7 days (V17, 20, 23), 14 days (V18, 21, 24) or 21 days (V19, 22, 25; expression: red –green-blue codes for high-intermediate-low); B) D-clusters of the SOM defining gene sets S1-S7 with differential regulation among the samples; C) Expression score of the gene sets S1-S7 for all samples (expression: blue-brown codes for low-high; red frame indicating the samples further analyzed in Fig. 10).

4.3 Validation of Affymetrix chip data by quantitative real-time PCR

Comparative gene expression analysis by Affymetrix chips and RT-PCR confirmed the significant up-regulation of the degradation markers POSTN and MMP13 in 2nd LB (from S6; Fig. 10C, D). In contrast, the matrix regeneration markers DPT and PENK were only numerically upregulated

in 2nd LB according to the RT-PCR. However, there was a significant down-regulation of the wound healing marker ICAM 1 (from S7) in 2nd LB in the PCR results (Fig. 10C, D). The significantly increased expression of the connective tissue markers collagens 1, 3, and 5 alpha 1 (2nd LB > normal cartilage by Affymetrix) was partially confirmed, and the lack of significant differences between 2nd LB and normal cartilage for the cartilage markers collagens 2 alpha 1 and 9 alpha 2 was fully confirmed by RT-PCR. Also, the numerical increase of the cartilage marker ACAN in normal cartilage by Affymetrix was confirmed as a significant increase by RT-PCR (Fig. 10C, D).

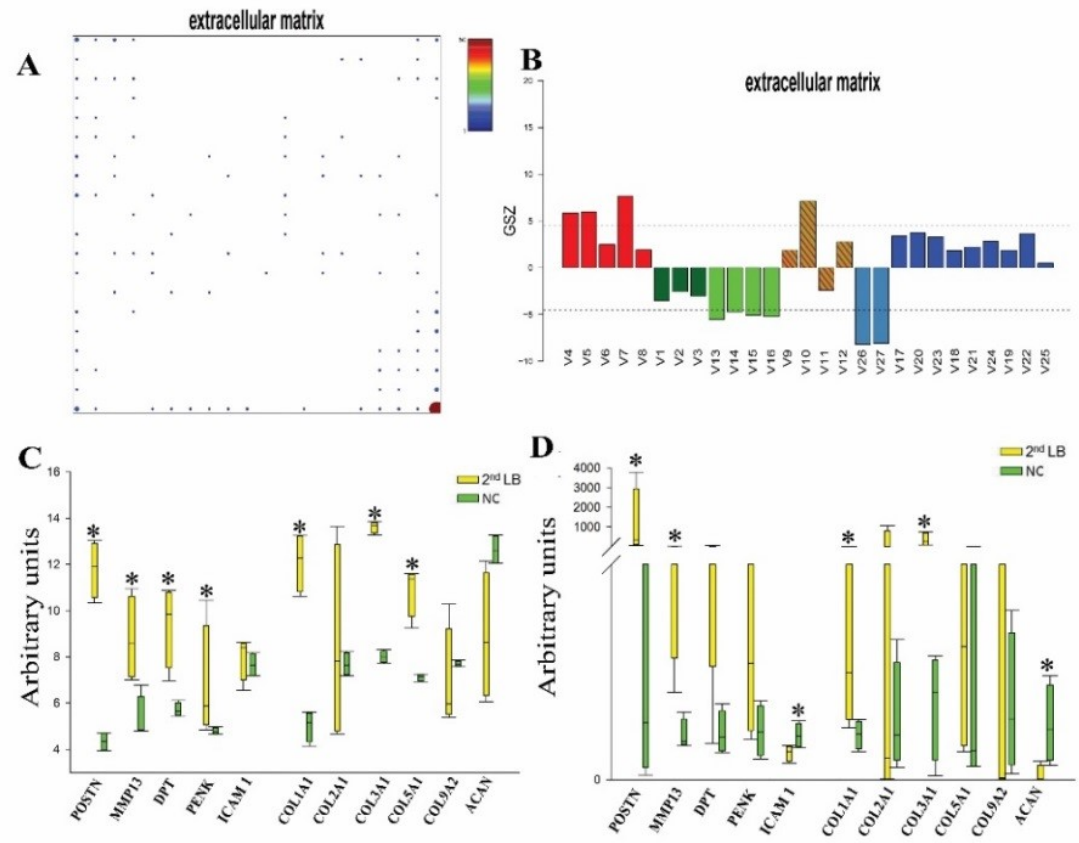

Figure 10: Gene expression details (normal cartilage V13-16; 2nd LB V9-V12): A) The GO gene set 'extracellular matrix' is closely related to subset S6, with 47/141 genes (33%) being part of S6 in the lower right metagene (20 x 20; compare with Fig. 9B); B) GSZ-score expression of the gene set 'extracellular matrix' for all samples (compare with Fig. 9C); C, D) Comparison of single gene expression based on Affymetrix chips (C) and RT-PCR (D); values are shown as medians ± 25th/75th percentiles (boxes) and 5th/95th percentiles (whiskers); *P ≤ 0.05 versus normal cartilage; POSTN=periostin; MMP13=matrix metalloprotease 13; DPT=dermatopontin; PENK= proenkephalin; ICAM 1=intercellular adhesion molecule 1;COL1A1, COL2A1, COL3A1, COL5A1, and COL9A2=alpha 1 and 2 chains, respectively, of collagens 1, 2, 3, 5, and 9; ACAN=aggrecan.

4.4 Constitutive frequency of different periostin isoforms in OA chondrocytes

All eight periostin isoforms were identified with different size PCR products in OA chondrocytes using primers widely spanning the periostin sequence (total periostin; E6 to E22; see Fig. 4 on page 17; Fig. 11A). Frequency analysis of each isoform by cloning resulted in high frequencies of approx. 30% for isoforms 3, 4, and 5, but lower frequencies for isoforms 1, 2, 6, 7, and 8 (≤ 3%; Fig. 11B). This was partially confirmed by isoform-specific RT-PCR (Fig. 4), resulting in frequencies ≥ 23% for isoforms 3, 4, 5, and 7, but ≤ 2% for isoforms 1, 2, 6, and 8 (Fig. 11C).

4.5 Silencing of different periostin isoforms with the siRNA construct G05

Qualitative analysis of the effects of periostin siRNA construct G05 (targeted to the isoforms 1, 2, 3, 4, 5, 8; see Table 2 on page 17) on OA chondrocytes by gel electrophoresis showed a clear weakening of the gel bands for the isoforms 5/8 and 3/2, but a relative sparing of the bands for the isoforms 1, 4/6, and 7 on days 2 and 4 (Fig. 11D). This was largely confirmed by a numerical downregulation of the PCR signal for total periostin (1 outlier) and isoforms 2, 4, and 6, as well as a significant downregulation of isoforms 2, 5, and 8 on day 2 (Fig. 11F). On day 4, the isoform downregulation was still maintained, with significantly reduced signals for total periostin and isoforms 3 and 8, and numerically reduced levels for isoforms 2, 5, and, in part, 7 (Fig. 11 G).

4.6 Silencing of the different periostin isoforms with the siRNA construct A02

The periostin siRNA construct A02 (targeted to all eight isoforms; Table 2) led to a complete disappearance of all gel bands on day 2, but a gradual return of all bands on day 4 (Fig. 11E). This was confirmed by a significant or numerical downregulation of the PCR signals for total periostin and all isoforms on day 2 ($P \leq 0.05$ for total periostin and isoforms 2, 3, 5, 6, 7, and 8; Fig. 11H) and on day 4 ($P \leq 0.05$ for total periostin and isoforms 2, 3, 7, and 8; Fig. 11I).

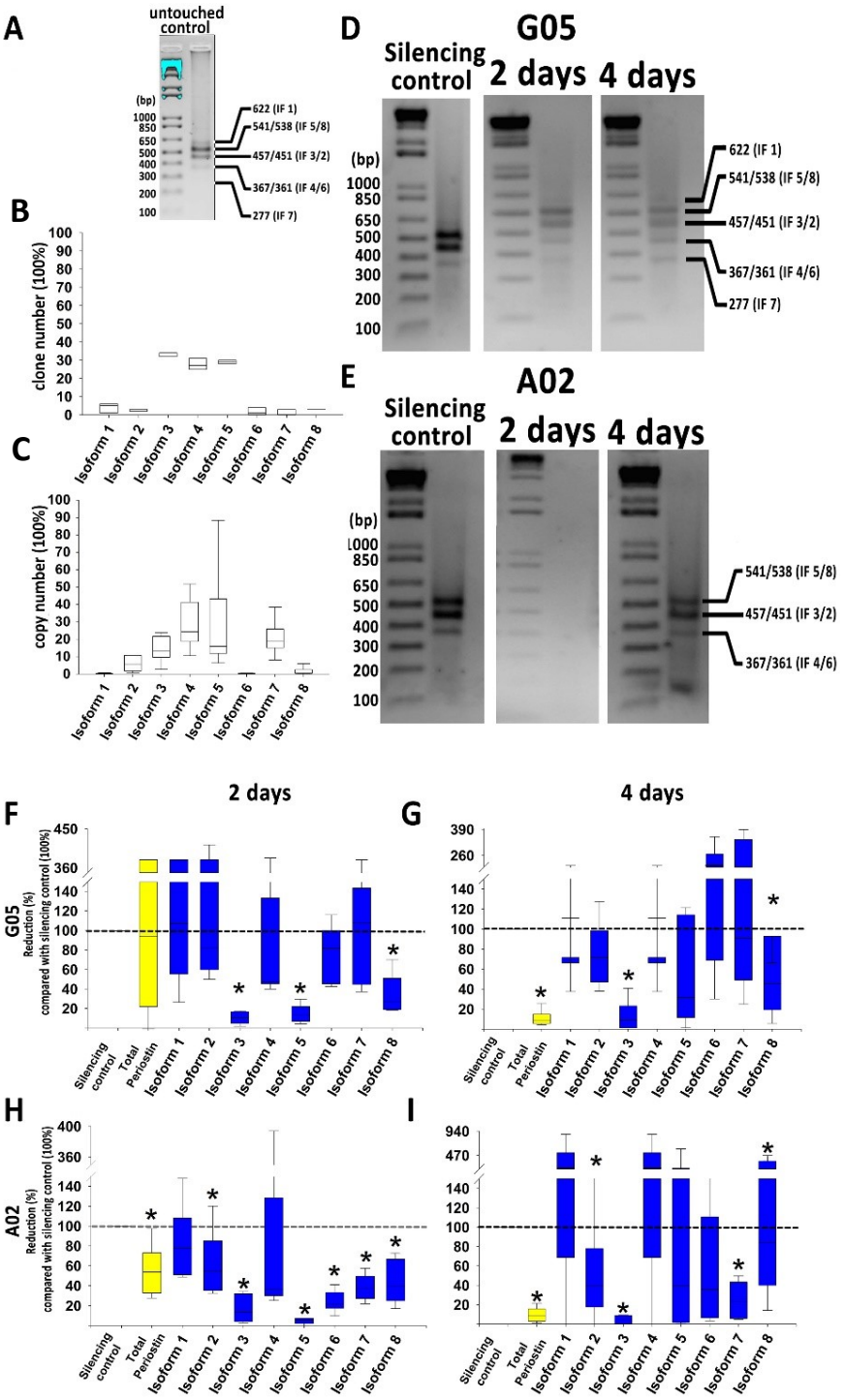

Figure 11: Constitutive frequency of different periostin isoforms in OA chondrocytes, as assessed by SDS gels (A), cloning (B), and isoform-specific PCR (C). Effects of silencing with the siRNA constructs G05 and A02, as assessed by SDS gels (D, E), and isoform-specific PCR (F-I); *P ≤ 0.05 versus silencing control.

4.7 Effects of periostin silencing on the expression of target genes of periostin

Periostin silencing with the siRNA constructs G05 and A02 led to a transient, numerical or significant downregulation of the expression of the periostin target gene MMP13 on day 2 (to 80 and 55%, respectively; $P \leq 0.05$ versus silencing control for A02), with a subsequent return to baseline levels or above on day 4 (Fig. 12A, D).

There were no significant effects of periostin silencing with either of the siRNA constructs on the expression of MMP3 on days 2 or 4 (Fig. 12B, E).

In contrast to MMP13, interestingly, the target gene ICAM 1 was significantly upregulated by periostin silencing with both siRNA constructs on day 2 (2- and 5-fold, respectively) and in both cases remained numerically upregulated on day 4 (2- and 3-fold; respectively; Fig. 12C, F)

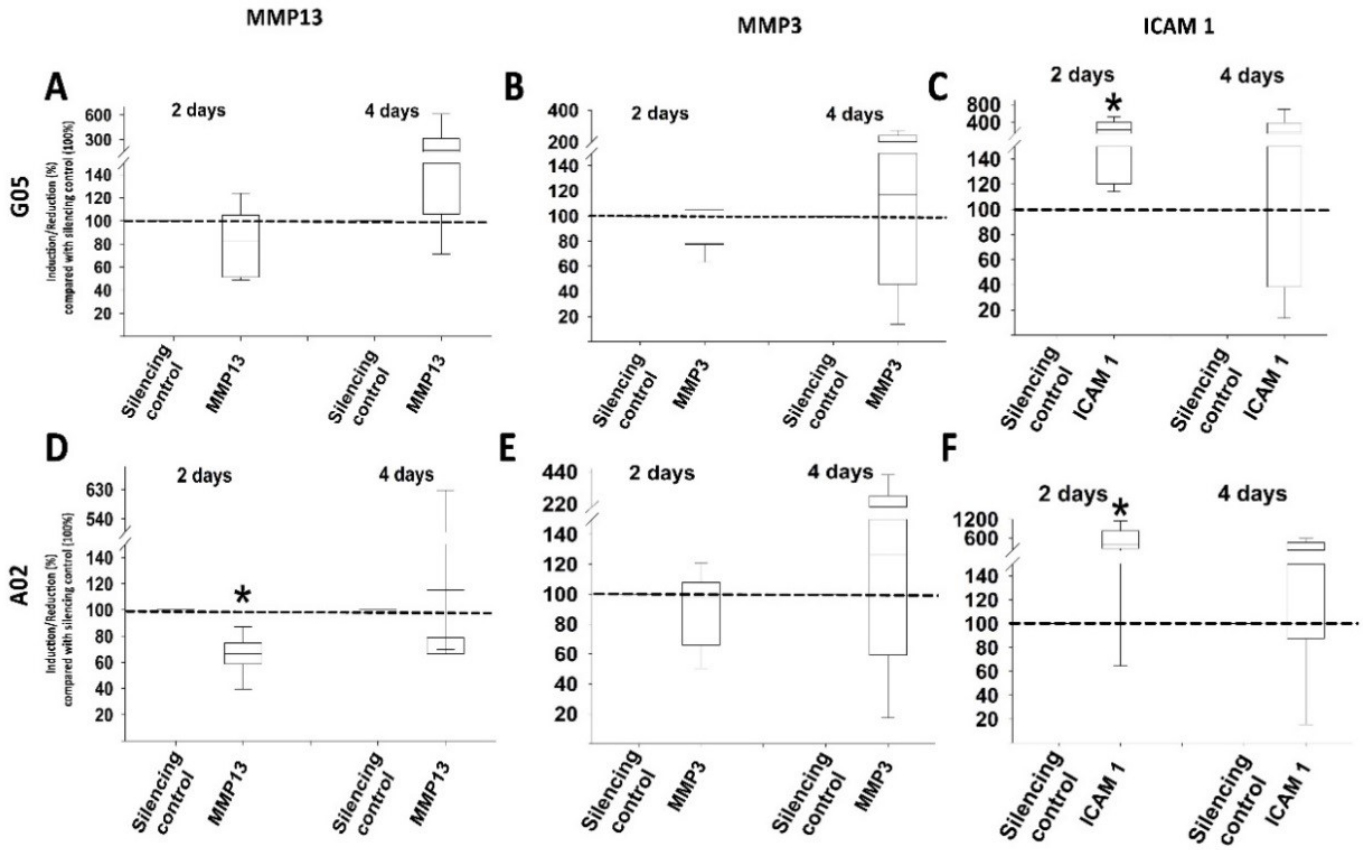

Figure 12: Effects of periostin silencing with the siRNA constructs G05 and A02 on the expression of MMP13 (A, D), MMP3 (B, E), and ICAM 1 (C, F), as assessed by PCR; the dashed line indicates the expression level of the respective gene in the silencing control samples (100%); *P ≤ 0.05 versus silencing control.

4.8 Effects of periostin silencing on the expression of marker genes

Periostin silencing with the siRNA constructs G05 and A02 led to a numerical or significant upregulation of the expression of the cartilage-specific marker gene COL 2, but also the bone and wound healing marker COL 3 on day 2 (3-fold and 1.1-fold, respectively; $P \leq 0.05$ versus silencing control for G05), which in both cases remained numerically upregulated on day 4 (3 fold and 5 - fold, respectively; Fig. 13A to D).

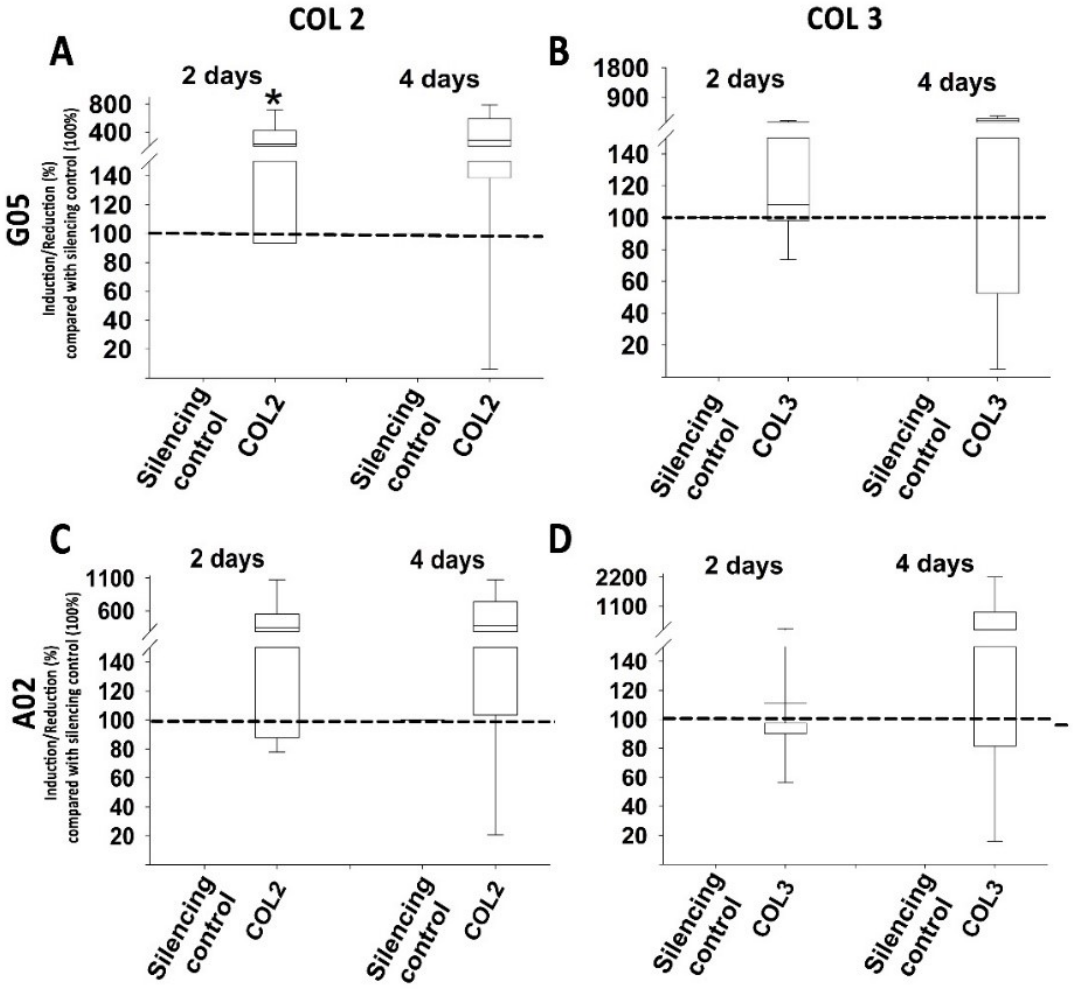

Figure 13: Effects of periostin silencing with the siRNA constructs G05 and A02 on the expression of COL 2 (A, C) and COL 3 (B, D; PCR); the dashed line indicates the expression level of the respective gene in the silencing control samples (100%); *$P \leq 0.05$ versus silencing control.

4.9 Effects of periostin silencing on the protein expression of periostin and MMP13

Periostin silencing with the siRNA constructs G05 and A02 led to a substantial, long-lasting, and significant suppression of the periostin protein levels in the supernatant of the silenced OA chondrocytes on days 2 and 4 (to 60 and 60 to 80%, respectively; $P \leq 0.05$ versus silencing control for both siRNA constructs on days 2 and 4; Fig. 14A).

Western blots confirmed a substantial reduction of the periostin protein levels in the cytoplasm of the silenced chondrocytes (shown for one representative patient; Fig. 14C).

In addition, periostin silencing with the siRNA construct G05 led to a transient and significant suppression of the MMP13 protein levels in the supernatant of the silenced OA chondrocytes on day 2 (to 90%; $P \leq 0.05$ versus silencing control; Fig. 14B), which was again largely confirmed in by Western blots in the cytoplasm of the silenced chondrocytes (Fig. 14C).

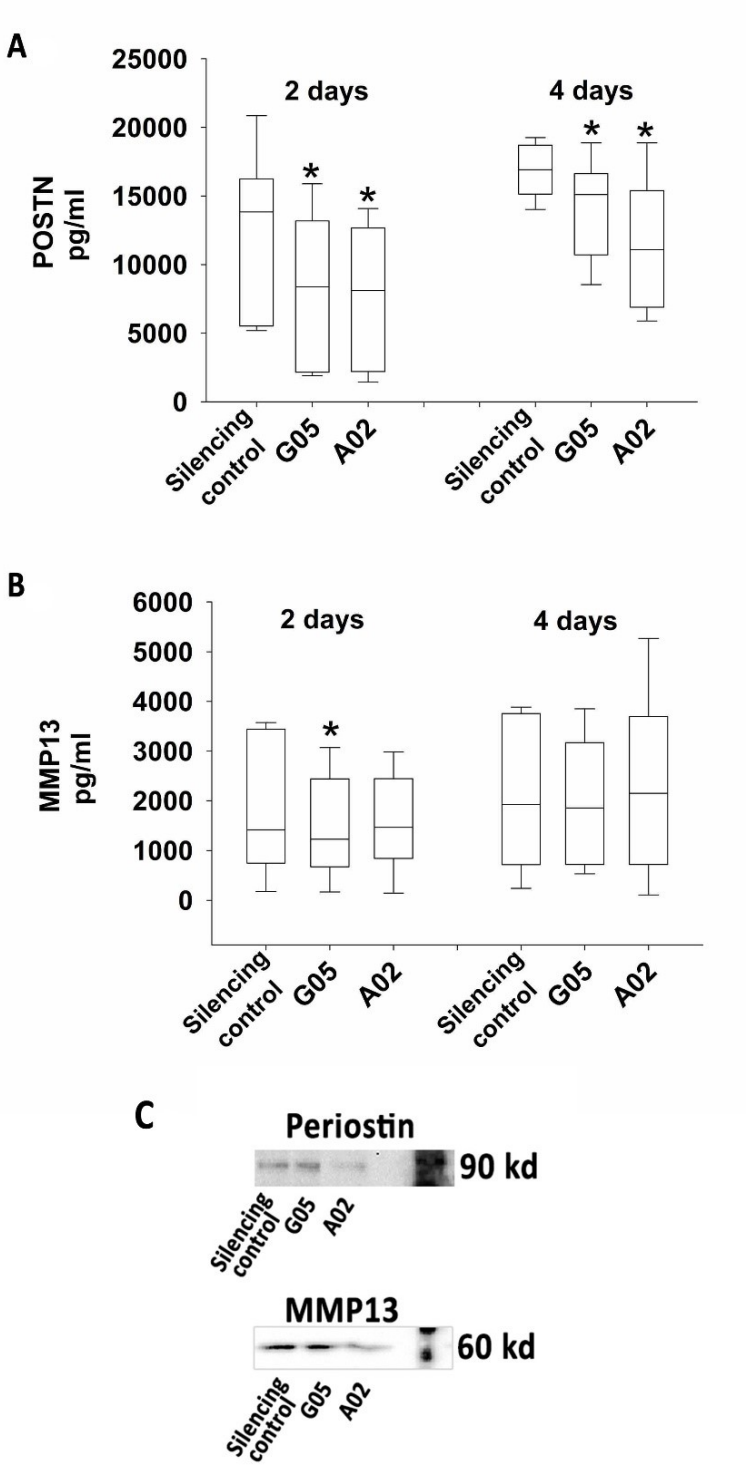

Figure 14: Effects of periostin silencing with the siRNA constructs G05 and A02 on the protein levels of periostin (A, C) and MMP13 (B, C) in the culture supernatant (A, B) and cytoplasm (C) of silenced OA chondrocytes (day 2), as assessed by ELISA (A, B) or Western blot (C); *P ≤ 0.05 versus silencing control.

5 DISCUSSION

The aim of this project was to define biomarkers and functional pathways for the optimization of chondrogenic differentiation in stem cell-based MACT. This was pursued by comparing 2nd LB from patients with MACT/cartilage repair procedures to normal cartilage on one hand, and to bone marrow-derived, human MSC differentiating into chondrocytes on the other hand. The focus of our studies were potential deficits (e.g., de- or mis-differentiation) of successful and functional cartilage repair following MACT. As a first step, biomarkers and pathways of chondrogenic differentiation were defined in cartilage regenerates after MACT by generating an atlas of differential gene expression between 2nd LB and normal cartilage, OA cartilage, or 3D-cultured chondrocytes using Affymetrix microarrays and SOM. The molecules/pathways underlying impaired cartilage repair were then validated by PCR and gene ontology analysis. The functional importance of the periostin-Wnt-MMP13 pathway was assessed by silencing of periostin in OA chondrocytes and the analysis of target and phenotype genes at the RNA and protein level. This approach aimed at evaluating the potential value of this pathway for the improvement of cartilage repair procedures.

The present study showed only limited similarity between 2nd LB and normal cartilage, and thus confirmed incomplete repair after cartilage replacement. On the other hand, similarities between 2nd LB and OA cartilage regarding the expression of inflammatory response genes suggested a contribution of inflammatory processes to the incomplete defect healing. Furthermore, the overexpression of matrix degradation and mis-differentiation markers, including the periostin-Wnt-MMP13 pathway, indicated molecular abnormalities accompanying insufficient cartilage repair. Indeed, successful counteraction (silencing) of periostin in OA chondrocytes led to transient downregulation of tissue-degrading MMP13 (mRNA and protein) and in upregulation of the cartilage marker collagen 2, pointing to a favorable effect of periostin silencing on the maintenance of the chondrogenic phenotype and the formation of mature cartilage. On the other hand, there was a transient upregulation of the wound healing markers ICAM 1 and collagen 3, raising the concern that downregulation of periostin may in parallel augment formation of wound healing and scar tissue.

5.1 Histological features of 2nd LB

The histology of the individual 2nd LB showed mixed features of connective tissue and cartilage, confirming previous results on the histological, immunohistological, and electron microscopy analysis of 2nd LB and 3rd LB [56-58]. This tissue heterogeneity did influence the patterns of gene expression in the individual 2nd LB (data not shown), but did not prevent the identification of relevant molecules/pathways potentially involved in deficits of successful and functional cartilage repair. Since the histology of 2nd LB will always depend on the surgeon's choice of tissue type and location, such heterogeneity is unavoidable and can only be balanced by including a higher number of samples [58]. However, the number of available 2nd LB is limited by the fact that second look re-arthroscopy following cartilage repair is only indicated upon complications such as persistent joint swelling and/or pain.

5.2 Identification of differentially expressed biomarkers/pathways of cartilage regeneration

Among other molecules/pathways, the periostin-Wnt-MMP13 pathway was identified by Affymetrix analyses and RT-PCR as one potentially relevant signaling pathways inhibiting the formation of fully mature regeneration cartilage. This is in agreement with previous publications on a potential role of periostin in matrix degradation and cartilage degeneration in OA [24, 59]. The Wnt pathway may also be also be targetable by non-toxic, small size chemical compounds such as CCT031374, which also inhibit the periostin induction of MMP13 expression [24], and may be usable instead of the complex, costly, and labor-intensive application of gene therapy approaches. Other differential clusters identified by Affymetrix arrays and SOM analysis included clusters containing markers of inflammation (S4), matrix interaction (S5), and the regulation of tissue architecture during wound healing (S7), providing the basis for future research concerning the promotion or suppression of cartilage regeneration.

5.3 Constitutive frequency of different periostin isoforms in OA chondrocytes

The present report for the first time showed a predominance of the isoforms 3, 4, 5, and 7 among the constitutively expressed periostin isoforms in OA chondrocytes. Some periostin isoforms appear to have specific functions during physiological or pathological tissue repair [26], cardiac remodeling [30], or lung embryogenesis [31], but there is currently no published information on the abundance or function of specific periostin isoforms in chondrocytes or cartilage. Future studies will have to compare the frequencies of periostin isoforms in normal and OA chondrocytes and possibly address specific isoform functions by directed silencing experiments.

5.4 Successful silencing of different periostin isoforms using different siRNA constructs

In partial agreement with the presumed periostin isoform targets of the siRNA constructs G05 (isoforms 1, 2, 3, 4, 5, 8) and A02 (all isoforms; see Fig 4), A02 led to a complete disappearance of all gel bands and a significant or numerical downregulation of the PCR signals for total periostin and all isoforms on day 2, whereas G05 showed a relative sparing of isoforms 6 and 7 on day 2 (gel electrophoresis; PCR). This shows that the targeting of specific periostin isoforms is in principal possible, although due to possible interactions among the isoforms and the complex structure of exon-exon junctions in different periostin isoforms RNA silencing remains a complex molecular biological task (see Fig. 4).

In the cases of both siRNA constructs, there was a gradual return of the periostin isoform expression to base line levels, in agreement with the limited half-life of the siRNA constructs. This also shows that the total dose and timing of applied siRNA have to be carefully titered to obtain reproducible results (data not shown; [60]).

5.5 Effects of periostin silencing on the mRNA expression of periostin target genes

The successful transient suppression of MMP13 expression by periostin silencing confirms published data [24], whereas the significant upregulation of ICAM 1 and cartilage-specific collagen 2 are reported for the first time in the present study. This supports the view that isolated silencing of periostin may have favorable effects on the chondrogenic phenotype and the formation of mature cartilage, but at the same time may augment the formation of scar tissue, as indicated by the upregulation of the wound healing markers ICAM 1 (4-6-fold) and collagen 3 (1.1-10-fold). This can be addressed by either inhibiting the periostin-Wnt-MMP13 pathway more thoroughly by a combination of different techniques or compounds [24], or else by inhibiting other target molecules in the identified relevant pathways, either alone or in combination with periostin.

5.6 Effects of periostin silencing on the protein expression of periostin and MMP13

Periostin silencing with both siRNA constructs resulted in a substantial, long-lasting, and significant suppression of the periostin protein levels in the cytoplasm and supernatant of the silenced OA chondrocytes, with a partially stronger effect of the siRNA A02 construct targeting all periostin isoforms. This shows that the present experimental design was well suitable to address the aims and questions of this study.

On the other hand, the suppression of the MMP13 protein production was transient (day 2) and only effective after silencing with the siRNA construct G05. This again emphasizes the importance of the exact experimental design and choice of target molecules for RNA silencing.

6 CONCLUSIONS

In the present study, biomarkers and pathways of impaired chondrogenic differentiation were defined in cartilage regenerates after MACT/cartilage repair procedures by comparative gene expression analysis in 2nd LB and normal cartilage using Affymetrix microarrays and bioinformatics. Relevant target molecules/pathways were then validated by PCR and gene ontology analysis. The functional importance of the identified periostin-Wnt-MMP13 pathway was demonstrated by downstream effects of periostin silencing in OA chondrocytes on the chondrogenic phenotype and the formation of mature cartilage, but also on the concurrent formation of wound healing and scar tissue. This shows that the aims of the study can be pursued by the current combination of translational and cell biology methods. However, further refinement of the therapeutic molecular targets is necessary to improve cartilage repair and develop novel treatments for articular cartilage defects.

REFERENCES

1. Mithoefer K, McAdams TR, Scopp JM, Mandelbaum BR. Emerging options for treatment of articular cartilage injury in the athlete. Clin Sports Med 2009; 28: 25-40.
2. Bhosale AM, Richardson JB. Articular cartilage: structure, injuries and review of management. Br Med Bull 2008; 87: 77-95.
3. Fosang AJ, Beier F. Emerging Frontiers in cartilage and chondrocyte biology. Best Pract Res Clin Rheumatol 2011; 25: 751-766.
4. Dewan AK, Gibson MA, Elisseeff JH, Trice ME. Evolution of autologous chondrocyte repair and comparison to other cartilage repair techniques. Biomed Res Int 2014; 2014: 272481.
5. Goldring MB. Chondrogenesis, chondrocyte differentiation, and articular cartilage metabolism in health and osteoarthritis. Ther Adv Musculoskelet Dis 2012; 4: 269-285.
6. Correa D, Lietman SA. Articular cartilage repair: Current needs, methods and research directions. Semin Cell Dev Biol 2017; 62: 67-77.
7. Sophia Fox AJ, Bedi A, Rodeo SA. The basic science of articular cartilage: structure, composition, and function. Sports Health 2009; 1: 461-468.
8. Eyre D. Collagen of articular cartilage. Arthritis Res 2002; 4: 30-35.
9. Luo Y, Sinkeviciute D, He Y, Karsdal M, Henrotin Y, Mobasheri A, et al. The minor collagens in articular cartilage. Protein Cell 2017; 8: 560-572.
10. Buckwalter JA, Mankin HJ. Articular cartilage: tissue design and chondrocyte-matrix interactions. Instr Course Lect 1998; 47: 477-486.
11. Okamoto O, Fujiwara S. Dermatopontin, a novel player in the biology of the extracellular matrix. Connect Tissue Res 2006; 47: 177-189.
12. AJ SF, A B, SA R. - The basic science of articular cartilage: structure, composition, and function. - Sports Health. 2009 Nov;1(6):461-8. doi: 10.1177/1941738109350438.: - 461-468.
13. Kuettner KE, Cole AA. Cartilage degeneration in different human joints. Osteoarthritis Cartilage 2005; 13: 93-103.
14. Goldring MB. Articular Cartilage Degradation in Osteoarthritis. Hss j 2012; 8: 7-9.
15. Musumeci G, Loreto C, Carnazza ML, Martinez G. Characterization of apoptosis in articular cartilage derived from the knee joints of patients with osteoarthritis. Knee Surg Sports Traumatol Arthrosc 2011; 19: 307-313.
16. Lee AS, Ellman MB, Yan D, Kroin JS, Cole BJ, van Wijnen AJ, et al. A current review of molecular mechanisms regarding osteoarthritis and pain. Gene 2013; 527: 440-447.
17. Lane NE, Brandt K, Hawker G, Peeva E, Schreyer E, Tsuji W, et al. OARSI-FDA initiative: defining the disease state of osteoarthritis. Osteoarthritis Cartilage 2011; 19: 478-482.
18. Im HJ, Muddasani P, Natarajan V, Schmid TM, Block JA, Davis F, et al. Basic fibroblast growth factor stimulates matrix metalloproteinase-13 via the molecular cross-talk between the mitogen-activated protein kinases and protein kinase Cdelta pathways in human adult articular chondrocytes. J Biol Chem 2007; 282: 11110-11121.
19. Maldonado M, Nam J. The role of changes in extracellular matrix of cartilage in the presence of inflammation on the pathology of osteoarthritis. Biomed Res Int 2013; 2013: 284873.
20. Novakofski KD, Pownder SL, Koff MF, Williams RM, Potter HG, Fortier LA. High-Resolution Methods for Diagnosing Cartilage Damage In Vivo. Cartilage 2016; 7: 39-51.
21. Murphy G, Lee M. What are the roles of metalloproteinases in cartilage and bone damage? Ann Rheum Dis 2005; 64: iv44-47.

22. Gendron C, Kashiwagi M, Lim NH, Enghild JJ, Thogersen IB, Hughes C, et al. Proteolytic activities of human ADAMTS-5: comparative studies with ADAMTS-4. J Biol Chem 2007; 282: 18294-18306.
23. Rose BJ, Kooyman DL. A Tale of Two Joints: The Role of Matrix Metalloproteases in Cartilage Biology. Dis Markers 2016; 2016: 4895050.
24. Attur M, Yang Q, Shimada K, Tachida Y, Nagase H, Mignatti P, et al. Elevated expression of periostin in human osteoarthritic cartilage and its potential role in matrix degradation via matrix metalloproteinase-13. Faseb j 2015; 29: 4107-4121.
25. Liu AY, Zheng H, Ouyang G. Periostin, a multifunctional matricellular protein in inflammatory and tumor microenvironments. Matrix Biol 2014; 37: 150-156.
26. Conway SJ, Izuhara K, Kudo Y, Litvin J, Markwald R, Ouyang G, et al. The role of periostin in tissue remodeling across health and disease. Cell Mol Life Sci 2014; 71: 1279-1288.
27. Kudo A, Kii I. Periostin function in communication with extracellular matrices. J Cell Commun Signal 2018; 12: 301-308.
28. Bai Y, Nakamura M, Zhou G, Li Y, Liu Z, Ozaki T, et al. Novel isoforms of periostin expressed in the human thyroid. Jpn Clin Med 2010; 1: 13-20.
29. Gadermaier E, Tesarz M, Suciu AA, Wallwitz J, Berg G, Himmler G. Characterization of a sandwich ELISA for the quantification of all human periostin isoforms. J Clin Lab Anal 2018; 32.
30. Morita H, Komuro I. Periostin Isoforms and Cardiac Remodeling After Myocardial Infarction: Is the Dispute Settled? Hypertension 2016; 67: 504-505.
31. Morra L, Rechsteiner M, Casagrande S, von Teichman A, Schraml P, Moch H, et al. Characterization of periostin isoform pattern in non-small cell lung cancer. Lung Cancer 2012; 76: 183-190.
32. Chijimatsu R, Kunugiza Y, Taniyama Y, Nakamura N, Tomita T, Yoshikawa H. Expression and pathological effects of periostin in human osteoarthritis cartilage. BMC Musculoskelet Disord 2015; 16.
33. Zeng L, Rong XF, Li RH, Wu XY. Icariin inhibits MMP1, MMP3 and MMP13 expression through MAPK pathways in IL1betastimulated SW1353 chondrosarcoma cells. Mol Med Rep 2017; 15: 2853-2858.
34. Okamoto O, Fujiwara S, Abe M, Sato Y. Dermatopontin interacts with transforming growth factor beta and enhances its biological activity. Biochem J 1999; 337 (Pt 3): 537-541.
35. Nagui NA, Ezzat MA, Abdel Raheem HM, Rashed LA, Abozaid NA. Possible role of proenkephalin in psoriasis. Clin Exp Dermatol 2016; 41: 124-128.
36. Ashour N, Angulo JC, Andres G, Alelu R, Gonzalez-Corpas A, Toledo MV, et al. A DNA hypermethylation profile reveals new potential biomarkers for prostate cancer diagnosis and prognosis. Prostate 2014; 74: 1171-1182.
37. Roperch JP, Incitti R, Forbin S, Bard F, Mansour H, Mesli F, et al. Aberrant methylation of NPY, PENK, and WIF1 as a promising marker for blood-based diagnosis of colorectal cancer. BMC Cancer 2013; 13: 566.
38. Davies ME, Dingle JT, Pigott R, Power C, Sharma H. Expression of intercellular adhesion molecule 1 (ICAM-1) on human articular cartilage chondrocytes. Connect Tissue Res 1991; 26: 207-216.
39. Deng Z, Jin J, Zhao J, Xu H. Cartilage Defect Treatments: With or without Cells? Mesenchymal Stem Cells or Chondrocytes? Traditional or Matrix-Assisted? A Systematic Review and Meta-Analyses. Stem Cells Int 2016; 2016: 9201492.
40. Huang BJ, Hu JC, Athanasiou KA. Cell-based tissue engineering strategies used in the clinical repair of articular cartilage. Biomaterials 2016; 98: 1-22.
41. Kon E, Filardo G, Di Matteo B, Perdisa F, Marcacci M. Matrix assisted autologous chondrocyte transplantation for cartilage treatment: A systematic review. Bone Joint Res 2013; 2: 18-25.

42. Brittberg M. Cellular and Acellular Approaches for Cartilage Repair: A Philosophical Analysis. Cartilage 2015; 6: 4s-12s.
43. Yin L, Wu Y, Yang Z, Denslin V, Ren X, Tee CA, et al. Characterization and application of size-sorted zonal chondrocytes for articular cartilage regeneration. Biomaterials 2018; 165: 66-78.
44. Arthroscopic Lavage and Debridement for Osteoarthritis of the Knee: An Evidence-Based Analysis. Ont Health Technol Assess Ser 2005; 5: 1-37.
45. Muller S, Breederveld RS, Tuinebreijer WE. Results of Osteochondral Autologous Transplantation in the Knee. Open Orthop J 2010; 4: 111-114.
46. Brittberg M, Gomoll AH, Canseco JA, Far J, Lind M, Hui J. Cartilage repair in the degenerative ageing knee: A narrative review and analysis. Acta Orthop 2016; 87: 26-38.
47. HB S, MJ K, EC M. - Matrix-Assisted Autologous Chondrocyte Transplantation in the Knee: A Systematic. - Orthop J Sports Med. 2017 Jun 6;5(6):2325967117709250. doi: : - 2325967117709250.
48. Schinhan M, Gruber M, Dorotka R, Pilz M, Stelzeneder D, Chiari C, et al. Matrix-associated autologous chondrocyte transplantation in a compartmentalized early stage of osteoarthritis. Osteoarthritis Cartilage 2013; 21: 217-225.
49. Karlsson C, Dehne T, Lindahl A, Brittberg M, Pruss A, Sittinger M, et al. Genome-wide expression profiling reveals new candidate genes associated with osteoarthritis. Osteoarthritis Cartilage 2010; 18: 581-592.
50. Kaps C, Frauenschuh S, Endres M, Ringe J, Haisch A, Lauber J, et al. Gene expression profiling of human articular cartilage grafts generated by tissue engineering. Biomaterials 2006; 27: 3617-3630.
51. Grosset AA, Loayza-Vega K, Adam-Granger E, Birlea M, Gilks B, Nguyen B, et al. Hematoxylin and Eosin Counterstaining Protocol for Immunohistochemistry Interpretation and Diagnosis. Appl Immunohistochem Mol Morphol 2017.
52. Lu K, Shi T, Li L, Zhang K, Zhu X, Shen S, et al. Zhuangguguanjie formulation protects articular cartilage from degeneration in joint instability-induced murine knee osteoarthritis. Am J Transl Res 2018; 10: 411-421.
53. Gautier L, Cope L, Bolstad BM, Irizarry RA. affy--analysis of Affymetrix GeneChip data at the probe level. Bioinformatics 2004; 20: 307-315.
54. Loffler-Wirth H, Kalcher M, Binder H. oposSOM: R-package for high-dimensional portraying of genome-wide expression landscapes on bioconductor. Bioinformatics 2015; 31: 3225-3227.
55. Livak KJ, Schmittgen TD. Analysis of relative gene expression data using real-time quantitative PCR and the 2(-Delta Delta C(T)) Method. Methods 2001; 25: 402-408.
56. Brun P, Dickinson SC, Zavan B, Cortivo R, Hollander AP, Abatangelo G. Characteristics of repair tissue in second-look and third-look biopsies from patients treated with engineered cartilage: relationship to symptomatology and time after implantation. Arthritis Res Ther 2008; 10: R132.
57. Loken S, Ludvigsen TC, Hoysveen T, Holm I, Engebretsen L, Reinholt FP. Autologous chondrocyte implantation to repair knee cartilage injury: ultrastructural evaluation at 2 years and long-term follow-up including muscle strength measurements. Knee Surg Sports Traumatol Arthrosc 2009; 17: 1278-1288.
58. DiBartola AC, Everhart JS, Magnussen RA, Carey JL, Brophy RH, Schmitt LC, et al. Correlation between histological outcome and surgical cartilage repair technique in the knee: A meta-analysis. Knee 2016; 23: 344-349.
59. Tajika Y, Moue T, Ishikawa S, Asano K, Okumo T, Takagi H, et al. Influence of Periostin on Synoviocytes in Knee Osteoarthritis. In Vivo 2017; 31: 69-77.
60. Bartlett DW, Davis ME. Insights into the kinetics of siRNA-mediated gene silencing from live-cell and live-animal bioluminescent imaging. Nucleic Acids Res 2006; 34: 322-333.

Appendix

List of Figures

List of Tables

Acknowledgments

First, I would like to thank the Graduate Academy of the Friedrich Schiller University Jena for awarding me the scholarship for my doctoral studies. I express my immense gratitude to my supervisor Prof. Dr. Raimund W. Kinne for his scientific rigor and support. My special thanks go to Prof. Dr. Regine Heller for giving me the chance to come to Jena. I am very grateful to Mrs. Ukena Bärbel for her guidance in all the experimental procedures.

I thank Prof. Dr. Georg Matziolis, Dr. Stefan Pietsch, and Dr. Lars Bischoff at the Waldkrankenhaus “Rudolf Elle”, Eisenberg, for providing patient material for this work.

Thanks to all my friends and cousins Sudhir, Prabodh, Suneeta – for the moral support and great encouragement in everyday life and greatest thanks to my parents.

Finally, I would like to thank all my colleagues at the Waldkrankenhaus “Rudolf Elle”, Eisenberg for their help and support.

Curriculum Vitae

Personal data	
Name	Pavan Kumar
Surname	Kalla
Address	Lutherstraße 56
Telephone No.	+49 17665696185
E-mail	Pavankumar_kalla@yahoo.com
Date of birth	02.05.1989
Place of birth	Visakhapatnam- India

Academic education and degrees	**Duration**
Doctoral Studies Faculty of Medicine Friedrich Schiller University Jena, Germany	03/2015-present
M.Sc Biotechnology Bangalore University.	09/2010-08/2012
B.Sc Biotechnology Andhra University	06/2007-04/2010

Working and research experience	**Duration**
Jena University Hospital, PhD researcher Experimental Rheumatology Unit Faculty of Medicine	03/2014-present
TRIMS (Research assistant) (Translational research) Visakhapatnam A.P, India	03/2012-09/2012
Indian academy (Part time) **(**Translational research) Bangalore Karnataka, India	02/2013-08/2013

Language skills	**Level of proficiency**
Telugu	mother tongue
English	proficient
Hindi	proficient
German	A2

Scholarship

- DAAD fellowship for the **Jena Summer School of Molecular Medicine** 2014.
- **Landesgraduiertenstipendien** for "New **Clin**ical biomarkers for **Ca**rtilage **Re**generation by **M**esenchymal Stem Cells (**ClinCaReM**)" from April 2015 to March 2018.

Poster presentations

- Poster Presentation on **'High-throughput analysis of the expression of wound healing markers in 2nd look biopsies after MACT'** at DKOU 2017.
- Poster Presentation on **'High-throughput analysis of gene expression in 2ndlook biopsies after MACT indicates incomplete/insufficient cartilage regeneration'** at DKOU 2016.

Research skills

- DNA, RNA & proteins handeling and analysis.
- Handling cell culture.
- Handling gas chromatography.
- experience in translational research and online bioinformatic tools.

Computer skills

- Macromedia Dream Weaver
- Adobe Photoshop
- Adobe illustrator
- Macromedia flash
- Developing web page layout
- MS Office
- Internet operation
- Basic C programming
- Corel Draw
- Chief Architecture

I hereby declare that the above-mentioned information is correct up to my knowledge and I bear the responsibility for the correctness of the above-mentioned particulars.

Place: Jena

Date: 4th of April 2018 **PAVAN KUMAR KALLA**

Sworn Statement

List of publications by candidate

The current work comprises the following research paper, which is ready for re-submission in recognized peer-review academic journals. The thesis is mainly based on the following paper:

Submitted journal manuscript

1. Kalla PK, Horbert V, Przybilla J, Kunisch, E, Koczan D, Pietsch S, Bischoff L, Dehne T, Ringe J, Galle J, Kinne RW. High-throughput analysis of gene expression in second-look biopsies after poor outcome matrix-assisted autologous chondrocyte transplantation indicates incomplete cartilage regeneration (ready for re-submission to osteoarthritis and cartilage).

Published posters

1. Kalla PK, Horbert V, Przybilla J, Kunisch, E, Koczan D, Pietsch S, Bischoff L, Dehne T, Ringe J, Galle J, Kinne RW. High-throughput analysis of gene expression in 2nd look biopsies after MACT indicates incomplete/insufficient cartilage regeneration. Deutscher Kongress für Orthopädie und Unfallchirurgie, October 25-28, 2016, Berlin, Germany
2. Kalla PK, Horbert V, Przybilla J, Kunisch, E, Koczan D, Pietsch S, Bischoff L, Dehne T, Ringe J, Galle J, Kinne RW. High-throughput analysis of the expression of wound healing markers in 2nd look biopsies after MACT. Deutscher Kongress für Orthopädie und Unfallchirurgie, October 24-27, 2017, Berlin, Germany

Jena, 4th of April, 2018 **PAVAN KUMAR KALLA**

Ehrenwörtliche Erklärung

Hiermit erkläre ich, dass mir die Promotionsordnung der Medizinischen Fakultät der FriedrichSchiller-Universität bekannt ist,

ich die Dissertation selbst angefertigt habe und alle von mir benutzten Hilfsmittel, persönlichen Mitteilungen und Quellen in meiner Arbeit angegeben sind,

mich folgende Personen bei der Auswahl und Auswertung des Materials sowie bei der Herstellung des Manuskripts unterstützt haben, Prof. Dr. med. R. W. Kinne,

die Hilfe eines Promotionsberaters nicht in Anspruch genommen wurde und dass Dritte weder unmittelbar noch mittelbar geldwerte Leistungen von mir für Arbeiten erhalten haben, die im Zusammenhang mit dem Inhalt der vorgelegten Dissertation stehen,

dass ich die Dissertation noch nicht als Prüfungsarbeit für eine staatliche oder andere wissenschaftliche Prüfung eingereicht habe und

dass ich die gleiche, eine in wesentlichen Teilen ähnliche oder eine andere Abhandlung nicht bei einer anderen Hochschule als Dissertation eingereicht habe.

Jena, 09th April 2018 Pavan Kumar Kalla